Outdoor Soiling Loss Characterization and Statistical Risk Analysis of Photovoltaic Power Plants

by

Sravanthi Boppana

A Thesis Presented in Partial Fulfillment
of the Requirements for the Degree
Master of Science

Approved April 2015 by the
Graduate Supervisory Committee:

Govindasamy Tamizhmani, Chair
Devarajan Srinivasan
Bradley Rogers

ARIZONA STATE UNIVERSITY
May 2015

ABSTRACT

Two Masters Students, Sravanthi Boppana and Vidyashree Rajasekar jointly performed the indoor and outdoor soiling studies. This thesis presents the outdoor soiling study, whereas the other thesis presents the indoor soiling study. Similarly, the statistical risk analyses of two power plants were jointly performed by these two Masters students. Both power plants are located at the same cold-dry climate but one power plant carries framed modules and the other carries frameless modules. This thesis presents the results on the framed modules.

This is a two-part thesis:

Part 1 characterizes soiling losses using various techniques to understand the effect of soiling on photovoltaic modules. The higher the angle of incidence (AOI), the lower will be the photovoltaic (PV) module performance. Our research group has already reported the AOI investigation for cleaned modules of five different technologies with air/glass interface. However, the modules that are installed in the field would invariably develop a soil layer with varying thickness depending on the site condition, rainfall and tilt angle. The soiled module will have the air/soil/glass interface rather than air/glass interface. This study investigates the AOI variations on soiled modules of five different PV technologies. It is demonstrated that AOI effect is inversely proportional to the soil density. In other words, the power or current loss between clean and soiled modules would be much higher at a higher AOI than at a lower AOI leading to excessive energy production loss of soiled modules on cloudy days, early morning hours and late afternoon hours. Similarly, the spectral influence of soil on the performance of the module was investigated through reflectance and transmittance measurements. It was observed that the reflectance and transmittances losses vary linearly with soil density variation and the 600-700 nm band was identified as an ideal band for soil density measurements.

Part 2 of this thesis performs statistical risk analysis for a power plant through FMECA (Failure Mode, Effect, and Criticality Analysis) based on non-destructive field techniques and count data of the failure modes. Risk Priority Number is used for the grading guideline for criticality analysis. The analysis was done on a 19-year-old power plant in cold-dry climate to identify the most dominant failure and degradation modes. In addition, a comparison study was done on the current power plant (framed) along with another 18-year-old (frameless) from the same climate zone to understand the failure modes for cold-dry climatic condition.

DEDICATION

This thesis work at is dedicated to my whole family: Sreedevi Boppana and Parameswara Rao Boppana (my parents), Madhukar Madhineni and Arati Madhineni (my aunt and uncle), and Sai Sowmya Boppana and Sudhakar Madhineni (my siblings) for their constant motivation, love and support throughout my Master's program.

ACKNOWLEDGEMENT

I would like to thank my thesis advisor, Dr. Govindasamy Tamizhmani, for this opportunity to work at ASU- PRL. His guidance and support throughout my thesis work is deeply appreciated. It was a real pleasure working with someone as knowledgeable, experienced and hardworking as he is.

I would also like to thank my committee members, Dr. Rogers and Dr. Srinivasan, for their time and help during my work.

In addition, I would like offer my thanks to Dr. Joseph Kuitche for his guidance and knowledge he imparted in the past years. I would like to thank staff and students at ASU- PRL. I am grateful to be able to work with a group of individuals, who are hardworking, helpful and fun-filled people, and made the whole time during the Master's program a great experience. My special thanks goes to my partner in the project, Vidyashree Rajasekar, for help, constant support and motivation during this period. I would also like to thank Sai Tatapudi, Sanjay Shrestha, Mohammad Naeem, Jaya Mallineni, Bulent Bicer, Christopher Raupp, Neelesh Umachandran, Matthew Chicca, and Mathan Kumar Moorthy.

Table Of Contents

List Of Tables vii
List Of Figures viii
Part 1: OUTDOOR SOILING LOSS CHARACTERIZATION 1
1.1. INTRODUCTION 2
1.1.1. Background 2
1.1.2. Statement of Problem 3
1.2. LITERATURE REVIEW 6
1.2.1. Outdoor Measurement Procedure of IEC 61853-2 Standard 6
1.2.2. Sandia National Laboratory Method 7
1.2.3. Angle of Incidence Loss estimation using PVSyst 8
1.3. METHODOLOGY 11
1.3.1. Test Setup 11
1.3.2. Procedure 16
1.3.2.1. Cleaned Module Characterization 18
1.3.2.2. Soiled Modules Characterizations 19
1.3.3. Angle Of Incidence Effect on PV Modules 21
1.3.4. Reflectance Measurement 23
1.3.5. Transmittance Measurement 24
1.4. RESULTS AND DISCUSSIONS 25
1.4.1. Effect of Soiling on Transmittance 25
1.4.2. Influence of soiling on Reflectance 27
1.4.3. Effect of Angle of Incidence on performance of Soiled Module 31
1.4.4. Modelling of Soiling Losses Due To Effect of Angle Of Incidence 37
1.5. CONCLUSION 41

PART 2: STATISTICAL RISK ANALYSIS FOR PHOTOVOLTAIC POWER PLANTS 43
2.1. INTRODUCTION 44
2.1.1. Background 44
2.1.2. Statement of Problem 45
2.2. LITERATURE REVIEW 47
2.2.1. Failure Modes and Degradation Modes 47
2.2.2. FMECA Technique 50
2.3. METHODOLOGY 52
2.3.1. Determination of Occurrence 52
2.3.2. Determination of Detection 53
2.3.3. Determination of Severity 54
2.4. RESULTS AND DISCUSSION 56
2.4.1. Safety Failures 57
2.4.2. Degradation Rate 58
2.4.3. Occurrence and Detectability 61
2.4.4. Severity 62
2.4.5. RPN Calculation 63
2.4.6. Comparison with Model J 67
2.5. CONCLUSION 71
REFERENCES 72
Appendix A 74
Standard Operating Procedure (SOP) for Dust Sampling Using Washable Lint Rollers 74
Appendix B 77
Standard Operating Procedure For Reflectance and Transmittance 77
Appendix C 90

LIST OF TABLES

Table 1: Superstrate/encapsulant/substrate material formulation for test modules 11

Table 2 Soil Density estimation using average reflectance loss over 600 – 700 nm band. 31

Table 3 Soil Density for five rounds of AOI measurements 32

Table 4 Summary of observations from AOI curve of soiled PV modules 37

Table 5 Failure/Degradation modes and mechanisms 49

Table 6 Occurrence determination 53

Table 7 Detection Determination 54

Table 8 Severity Determination 55

Table 9 Site description 56

Table 10 Electrical Parameters of Module 57

Table 11 Occurrence and Detectability 61

Table 12 RPN Calculation 64

Table 13 Site Specification 67

LIST OF FIGURES

Figure 1. Interface in case of cleaned and soiled modules 3

Figure 2. Angle of Incidence effect Summary - Cleaned and Soiled Modules 4

Figure 3 Solar PV Glass 12

Figure 4. HandHeld FieldSpec 4 Wide-Res spectroradiometer from ASD Inc 14

Figure 5 Reflectance Accessory 14

Figure 6 RCR - Transmittance accessory 15

Figure 7 Outdoor test setup for AOI measurements 16

Figure 8 Characterization Test Flow Chart 17

Figure 9 Soil Sampling Modules 20

Figure 10 Transmittance Measurement for 0.869 g/m^2 26

Figure 11 Transmittance loss Vs Soil Density 26

Figure 12 Cleaned module reflectance for all module technologies 27

Figure 13 Reflectance Spectrum for different soil densities for Mono Si module. 28

Figure 14 Delta Plot for Mono Si at different soil densities 29

Figure 15 Delta Plot for CdTe at different soil densities 30

Figure 16 Relative optical response for cleaned modules of five technologies. 32

Figure 17 Relative optical response for modules of five technologies when soil density is $0.016g/m^2$. 33

Figure 18 Relative optical response for modules of five technologies when soil density is $0.648g/m^2$. 34

Figure 19 Relative optical response for Mono Si as soil density varies. 35

Figure 20 Critical angle Vs. Soil Density 36

Figure 21 Relative Optical Response for cleaned and soiled module of SD 0.263 g/m^2 38

Figure 22 AOI related soiling Annual Energy losses - Phoenix 38

Figure 23 AOI related annual energy soiling losses for different locations using measured data 39

Figure 24 Grading PV Power Plant- Conceptual approach 45

Figure 25 Safety failure 58

Figure 26 String Level Degradation for Model JVA 59

Figure 27 Module Level Degradation 60

Figure 28 Model-JVA's safety failures and extrapolated degradation distribution 60

Figure 29 RPN - Module level for Model JVA 65

Figure 30 String Level RPN for Model JVA 65

Figure 31 Global String level RPN with all defects for Model JVA 66

Figure 33 Pareto Chart for Model J 69

Figure 34 Pareto Chart for Model JVA 69

PART 1: OUTDOOR SOILING LOSS CHARACTERIZATION

1.1. INTRODUCTION

1.1.1. Background

The performance of the photovoltaic system depends on a wide range of factors like the cell efficiency, performance of other balance of system components (BOS) that are internal to the system, and external factors like available irradiance, ambient temperature, etc. that can be dependent on the geographic location and conditions. Soiling is one such environmental factor that is often overlooked, considering its unpredictable nature and location specific effect on performance. Dust can be comprised of small amounts of pollen (vegetation, fungi, bacteria), human/animal cells, hair, carpet and textile fibers (sometimes termed microfibers), and, most commonly, organic minerals from geomorphic fallout such as sand, clay, or eroded limestone. Atmospheric dust (aerosols) is attributed to various sources, such as soil elements lifted by the wind (aeolian dust) volcanic eruptions, vehicle movement, and pollution [1] . Often, the effect of soiling is most pronounced in those locations where the usage of solar energy is more apropos, like in case of desert or semi-arid regions. The study by Salim et al. into long-term dust accumulation on a solar-village PV system near Riyadh (Saudi Arabia) indicated a 32% reduction, after 8 months, in performance of the solar array due to dust accumulation [2]. Average annual soiling loss can range between 1 - 6 % annually depending on the site and environmental conditions and can be as high as 27% at a specific time [3,4]. It is now important to understand the effect of soiling completely and thereby model the performance effect. This is, however, very complex considering the wide range of factors that influence the process of dust deposition.

1.1.2. Statement of Problem

A typical photovoltaic (PV) module with glass superstrate has the following interfaces: air/superstrate, superstrate/encapsulant and encapsulant/cell. [5, 6] In the case of soiled PV modules, the incident light is influenced by two additional interfaces of air/soil and soil/superstrate as shown in Fig. 1. Therefore, for a soiled module, reflections and transmittances change due to these interfaces depending on soil density and effects the short circuit current of the module. The surface roughness and antireflective coatings of the superstrates heavily influence the incident angle effect.

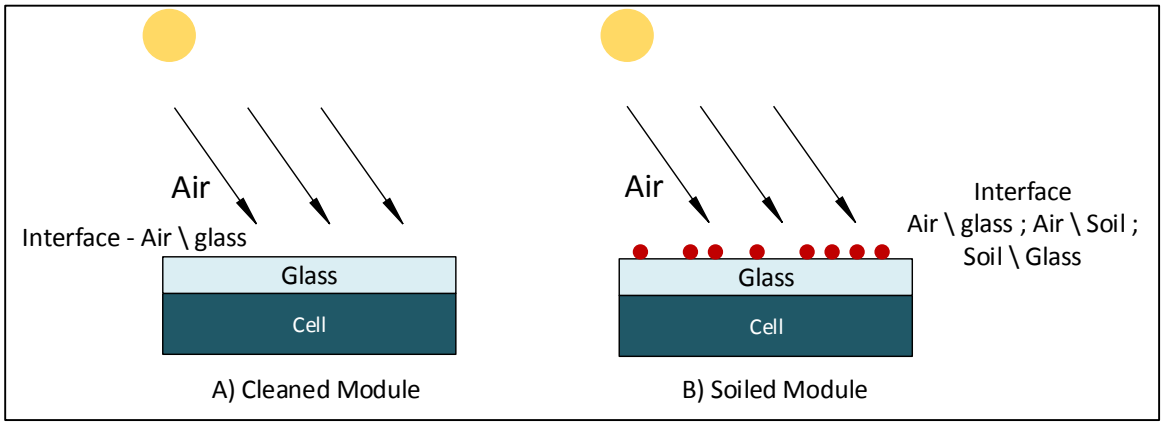

Figure 1. Interface in case of cleaned and soiled modules

Fig. 2 gives insight into the effect of the angle of incidence in a cleaned and soiled module. In a cleaned module, when the incident light is at 0° angle of incidence, there is little/no loss due to absorption and reflection on glass surface, whereas a soiled module experiences some absorption and reflection losses due to soiling. When the incident light is greater than 0° angle of incidence, there are Geometric losses or Cosine losses as well as Reflection loss [7]. The geometric losses are simply dependent on the angle at which the module is, with respect to incident light for a cleaned module, and can be calculated as the cosine of the angle of incidence. This remains the same in the case of a soiled

module. However, reflectance losses change for soiled modules from cleaned modules due to a change in interface structure. This phenomenon might be important in case of fixed tilt systems that experience a wide range of tilt angles.

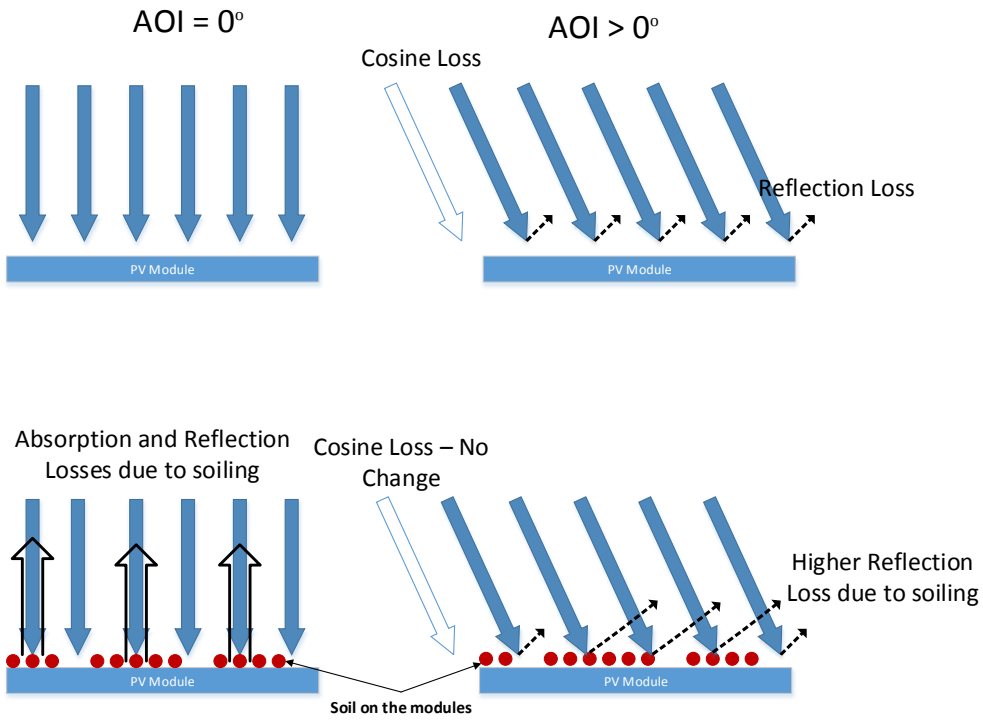

Figure 2. Angle of Incidence effect Summary - Cleaned and Soiled Modules

In this study, the reflectance, absorbance and angle of incidence related losses of soiled modules of five different technologies are investigated for field-soiled modules over a period of two months as the soil density varies. The five different module technologies used in this study are monocrystalline silicon (mono-Si), polycrystalline silicon (poly-Si), amorphous silicon (a-Si), cadmium telluride (CdTe), and copper indium gallium selenide (CIGS). The superstrate/encapsulant/substrate materials of these modules are respectively: glass/EVA/polymer (mono-Si); glass/EVA/polymer (poly-Si); glass/EVA/glass (a-Si); glass/EVA/glass (CdTe); glass/EVA/polymer (CIGS).

The angle of incidence effect measurement is performed following IEC 61853-2 and the relative optical response (f_2(AOI)) is measured following Sandia's method. This relative optical response is used in modelling performance losses as Incidence Angle Modifier (IAM) in performance modelling software such as PVSyst. The reflectance and transmittance losses due to soiling were performed using a portable spectroradiometer, thus making it possible to collect spectra, both indoors as well as in the field.

1.2. LITERATURE REVIEW

1.2.1. Outdoor Measurement Procedure of IEC 61853-2 Standard

IEC 61853-2 standard for measuring angle of incidence effects uses Isc data of the test modules corresponding to various angles of incidence [8]. This section includes a brief description of test apparatus, experimental setup, and measurement procedures followed for the current study.

Irradiance sensors are used to monitor the global and direct irradiance levels. A reference cell (using the shadowing/collimating method; refer to standard for a detailed procedure), or a combination of pyranometer for global irradiance and pyrheliometer for direct normal irradiance can be used. Thermal sensors are used to measure the ambient temperature and temperatures of test modules and reference cell. A data acquisition system collects and stores the output of thermal sensors, and the short circuit current of the test modules and output from irradiance sensors. Two-axis trackers are used to mount the test modules to be able to change the incident angles on the test modules. An AOI measuring device determines the tilt angle to the sun, and the co-planarity of test modules and irradiance sensors should be verified.

The diffuse component of irradiance should not exceed more than 10 % of the total global irradiance. The current study used pyranometer and pyrheliometer as irradiance sensors. The Equation (1) gives the diffuse component visible to the module.

$$G_{diff} = G_{tpoa} - G_{dni}\cos(\theta) \qquad (1)$$

Where G_{diff} is global diffuse irradiance,

G_{tpoa} is the total irradiance in the plane of the module (as measured by a pyranometer in the module plane),

G_{dni} is direct normal irradiance as measured by the pyrheliometer,

θ is tilt angle between the module normal and the direct solar irradiance i.e. angle of incidence.

Equation 2 gives the Isc generated from direct normal irradiance.

$$I_{SC}(\theta) = I_{sc_{measured}}(\theta)\left(1 - \frac{G_{diff}}{G_{tpoa}}\right) \qquad (2)$$

The relative angular light transmission (or relative angular optical response) into the module is given by Equation (3). This is measured for a minimum of nine angles of incidence ranging between 0 to 80°.

$$\tau(\theta) = \frac{I_{SC}(\theta)}{\cos(\theta) I_{SC}(0)} \qquad (3)$$

1.2.2. Sandia National Laboratory Method

Sandia National Laboratory's paper titled "Measuring Angle-of-Incidence (AOI) Influence on PV Module Performance" [7] presents a model for both mechanical and optical influences using an expanded expression to determine the effective solar irradiance. By taking into account the direct and diffused components of sunlight, the optical effect (f_2 (AOI)) can be measured empirically and calculated using the following Equations (4) and (5). For these equations to be valid, it is essential that the diffuse component is less than 10% during the experiment.

$$\mathrm{I_{scr}} = \mathrm{I_{sc}} * \left(\frac{\mathrm{E_o}}{\mathrm{E_{poa}}}\right) * \left(1 + \alpha_{\mathrm{Isc}}(\mathrm{T_c} - 25)\right) \qquad (4)$$

$$f_2(AOI) = \frac{\left[\mathrm{E_o} * \frac{\left(\frac{\mathrm{I_{sc}}}{1 + \alpha_{\mathrm{Isc}}(\mathrm{T_c} - 25)}\right)}{\mathrm{I_{scr}} - \left(\mathrm{E_{poa}} - \mathrm{E_{dni}} * \cos(\mathrm{AOI})\right)}\right]}{\left(\mathrm{E_{dni}} * \cos(\mathrm{AOI})\right)} \qquad (5)$$

Where:

Edni = Direct normal solar irradiance (W/m2)

Epoa = Global solar irradiance in the plane-of-array (module) (W/m2)

Eo = Reference global solar irradiance, typically 1000 W/m2

AOI = Angle between solar beam and module normal vector (deg)

Tc = Measured module (cell) temperature (°C)

α_{Isc} = Short-circuit current temperature coefficient (1/°C)

Isc = Measured short-circuit current (A)

The fifth order generic polynomial used to describe the typical optical response for modules with an air-glass interface was develop by Sandia Laboratories after empirical measurements for f_2(AOI) conventional flat-plate PV modules with planar glass-air interfaces were taken. This is given in Equation (6) below.

$$f2(AOI) = 1 - 2.4377E-3(AOI) + 3.1032E-4(AOI)^2 - 1.2458E-5(AOI)^3 + 2.1122E-7(AOI)^4 - 1.3593E-9(AOI)^5 \quad (6)$$

1.2.3. Angle of Incidence Loss estimation using PVSyst

Meteorological data

PVsyst includes a monthly Meteo database for about 1200 predefined stations of MeteoNorm (V 6.1 has been used in the current study) and monthly Meteo Data can be generated based on a MeteoNorm V 6.1 interpolating tool included in the PVsyst (1960-1990 or 1981-2000 averages) for locations not part of this database. PVSyst also accepts Meteo data from other sources like Satellight (Europe), US TMY2/3, and SolarAnywhere. Synthetic hourly data can be generated from monthly data for sites,

which do not have hourly data. The complete list of meteorological data sources and other details of on meteorological data is available on online PVSyst manual.

Irradiance Models

Transposition model or Plane of Array Irradiance models are used for calculation of incident irradiance on tilted array. The different components of irradiance i.e. beam or direct component, diffuse component and albedo component are calculated separately. The direct component is purely geometrical (cosine losses). Albedo is calculated as given fraction (the "albedo coefficient") of the global, weighted by the "orange slice" fraction defined between the horizontal and the tilted plane extension. Default albedo coefficients have been used. This study used Perez's Diffuse Irradiance Model in PVSyst.

Perez's Diffuse Irradiance Model

There are multiple diffuse Irradiance Models, but Perez's Model has been used, considering its widely accepted accuracy. The basic Equation 7 [13] gives the form of the model:

$$E_d = DHI * [(1 - F_1)\left(\frac{1+cos\theta_T}{2}\right) + F_1 * \frac{a}{b} + F_2 * sin\theta_T] \qquad (7)$$

Where

F_1 and F_2 are complex empirically fitted functions that describe circumsolar and horizon brightness, respectively

a=max (0, cos (AOI))

b=max (cos (85), cos (θ_Z))

DHI = diffuse horizontal irradiance

θ_z = solar zenith angle

$$F_1 = \max\left[0, \left(f_{11} + f_{12}\Delta + \frac{\pi\theta_z}{180°} f_{13}\right)\right]$$

$$F_2 = f_{21} + f_{22}\Delta + \frac{\pi\theta_z}{180^\circ} f_{13}$$

The f coefficients are defined for specific bins of clearness (ε), which is defined as:

$$\varepsilon = \frac{\frac{DHI + DNI}{DHI} + k\theta_z^3}{1 + k\theta_z^3}$$

Where,

k= 1.041 for angles are in radians (or 5.535 * 10^{-6} for angles in degrees)

$$\Delta = \frac{DHI * AM_a}{E_a}$$

Where, AM_a is the absolute air mass, and E_a is extraterrestrial radiation.

Incident Angle Modifier (IAM)

The angle of incidence loss is the decrease in irradiance that reaches the cell surface with respect to normal incident irradiance. In simpler words, it's the ratio of incident irradiance at a particular angle to that of zero angle of incidence. PVSyst uses the one parameter ASHRAE model, to estimate the IAM (Incidence Angle Modifier) at a particular tilt angle. However, this study uses Sandia's Polynomial for cleaned modules and the measured polynomial for soiled modules.

1.3. METHODOLOGY

1.3.1. Test Setup

The test apparatus, experimental setup and measurement procedure for characterization of soiling losses for field-soiled modules for the current study are as follows.

- *Test Modules*: Five modules of different technologies i.e. monocrystalline silicon (Mono-Si), polycrystalline silicon (Poly-Si), amorphous silicon (a-Si), cadmium telluride (CdTe), and copper indium gallium selenide (CIGS) were used in this study. Another polycrystalline silicon module was included in the setup to be used as a cleaned control module. All the test modules have glass superstrate, considering the first air/glass is the most influential parameter in AOI related losses.(brett). The superstrate/encapsulant/substrate material formulation for all the modules are listed in Table 1 below.

Table 1: Superstrate/encapsulant/substrate material formulation for test modules

Module Technology	superstrate/encapsulant/substrate material
Mono – Si	glass/EVA/polymer
Poly – Si	glass/EVA/polymer
a-Si	glass/EVA/glass
CdTe	glass/EVA/glass
CIGS	glass/EVA/polymer

These test modules were mounted on a two-axis tracker. A sundial was used to verify the coplanarity of the test modules as well as the control module before the test.

- *Solar PV Glass:* Two glass pieces were mounted on the tracker coplanar to the modules. A sundial was used to verify the coplanarity. One glass piece is left for soiling while the other is cleaned before every clean reading.

Figure 3 Solar PV Glass

- *Irradiance sensor:* The test employs a pyranometer (Kipp and Zonen) and a pyrheliometer (Epply) for plane of array irradiance and direct irradiance respectively. The pyranometer was mounted on the same test two-axis tracker, coplanar to the test modules, while the pyrheliometer was mounted on a second test tracker that continuously tracks the sun during the test duration.
- *Thermal sensor:* T-type thermocouples (Omega) were attached to the center of the backsheet of each module using a thermal tape. The accuracy of the thermocouples is given by the manufacturer as +/- 1°C or 0.75% for temperatures above 0°C.
- *Data measurement and Acquisition System*: A Daystar MT5 Multi-Tracer was used for measuring the short circuit current for the test modules. The system sweeps IV curves for all the test modules and stores this information along with the corresponding irradiance and temperature measurements. The multi curve tracer takes approximately

two seconds per module for IV measurement. All the measurements were taken under peak power tracking conditions. The system was placed in a temperature-controlled environment to ensure that the operating temperature does not exceed 50°C.

- AOI Measuring device- A 3DM-GX3-25 miniature attitude heading reference system from Microstrain was used to find the angle of incidence (AOI), i.e. the tilt of the modules and reference devices on the test tracker from the sun. It consists of a triaxial accelerometer, triaxial magnetometer, temperature sensors and processor that run an algorithm which provides static and dynamic orientation measurements with a manufacturer rated accuracy of +/- 0.5° static accuracy and a +/- 0.2° repeatability. The instrument was placed on a plastic arm attached to the tracker that is coplanar to the modules on the trackers. The angle of incidence was monitored and stored using a computer interface of the device as it is varied.

- Spectroradiometer – FieldSpec 4 Wide-Res spectroradiometer from ASD Inc. is a compact, portable, full-range (350-2500 nm) remote sensing Vis/NIR spectroradiometer with rapid data collection time of 0.2 second per spectrum. A spectroradiometer is an optical instrument for measuring the radiant energy from a source at each wavelength. The instrument is widely used for remote sensing and analysis of materials with broad spectral features. The instrument, along with the following accessories, was used for reflectance and transmittance measurements.

Figure 4. HandHeld FieldSpec 4 Wide-Res spectroradiometer from ASD Inc

1. *Reflectance accessory* - Hi-Brite Contact Probe from ASD Inc. was attached to the optical fiber of the spectroradiometer for reflectance measurements. The contact probe includes a halogen bulb light source and the optic fiber of the spectroradiometer measures this to give relative reflectance with respect to a white reference.

Figure 5 Reflectance Accessory

2. *Transmittance accessory* - For transmittance measurement, the spectroradiometer is fitted with a Remote Cosine Reflector (RCR) foreoptic, which enables full hemispherical absolute energy measurements. This allows the spectroradiometer to measure the total irradiance that is both direct irradiance and diffuse irradiance emitted by the sun, or an artificial light source, as well as the corresponding full

hemispherical reflectant radiance. This is used in the agricultural industry for understory characteristics and forestry applications for estimating total energy absorbed.

Figure 6 RCR - Transmittance accessory

- Two-axis tracker- All the modules, along with an irradiance sensor and an AOI measuring device, were mounted on a two-axis tracker. All the modules irradiance sensors and glass panels were set up in a coplanar manner. This was verified using a sundial. The two-axis tracker has a scope of 180° rotational angle in an azimuth angle and a 65° rotational angle in an elevation angle. This limits the highest AOI that can be achieved at a particular time-period. For the test time-period that is in the months of October and November, up to 80° AOI was possible when the experiment was conducted between 13:00 MST and 14:00 MST. However, data for AOI beyond 75° was excluded from the study due to albedo influence.
- Soil Sampling Module: An additional module, called soil-sampling module, was mounted on the tracker to collect soil samples to determine the soiling density. This was

essential, as soil density measurements on the test modules is not feasible in a continuous study. This module was placed coplanar to the test modules on the same 2-axis tracker, and was allowed to collect soil in the same conditions as the test modules, thereby making it represent the test modules.

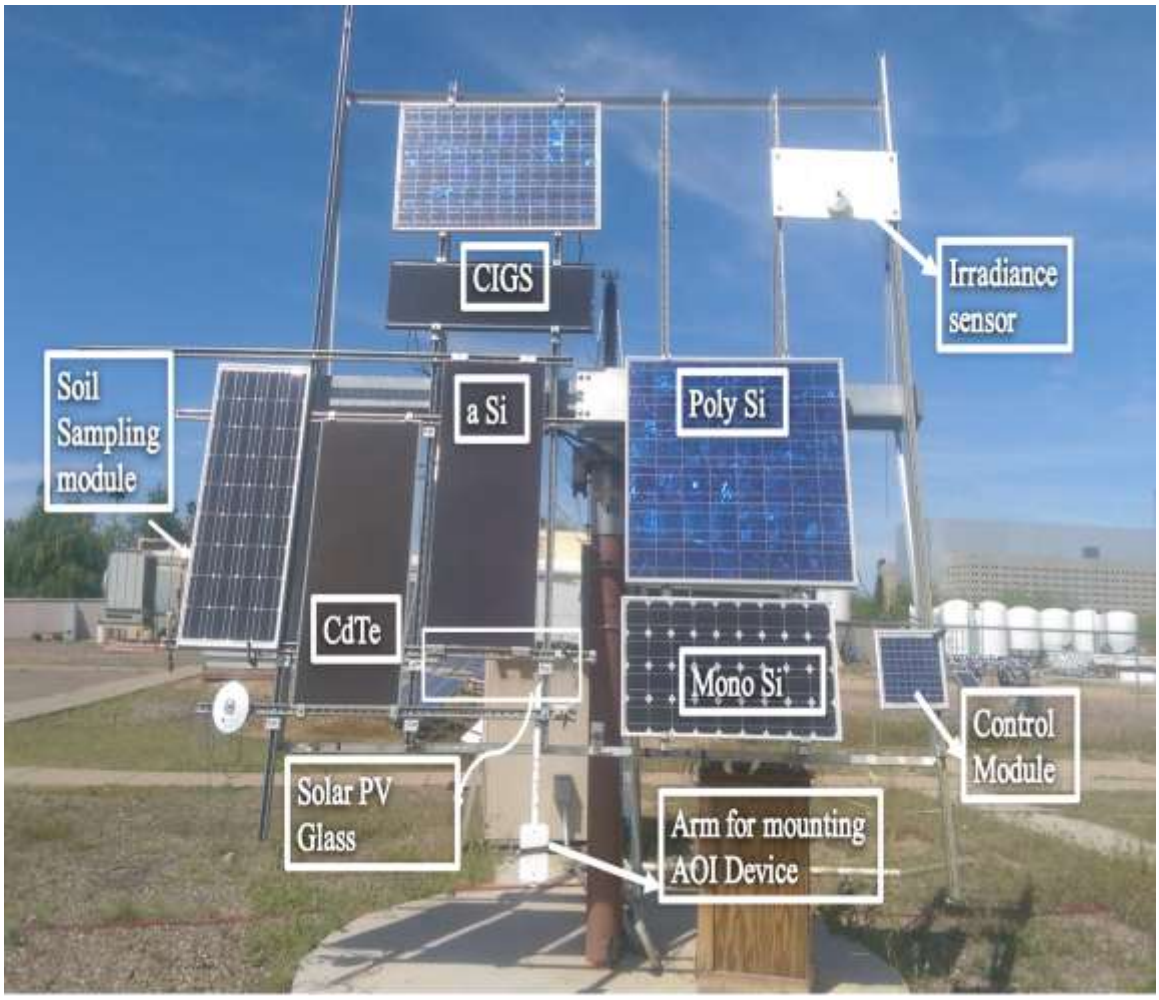

Figure 7 Outdoor test setup for AOI measurements

1.3.2. Procedure

The study involved performing AOI effect measurement, reflectance measurement and transmittance measurement for various soiling densities of field soiled modules as they naturally get soiled.

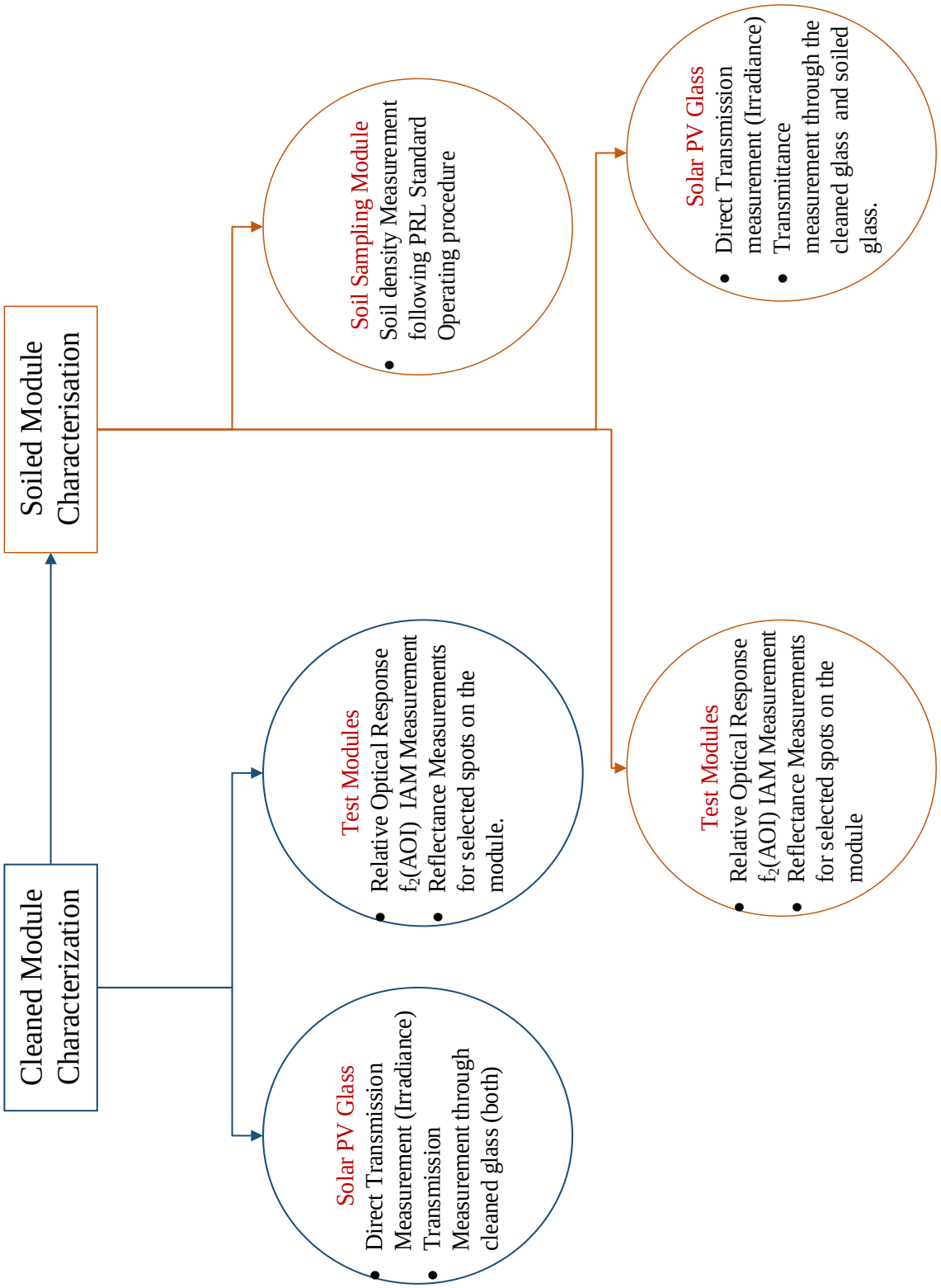

Figure 8 Characterization Test Flow Chart

1.3.2.1.Cleaned Module Characterization

Cleaned Module Characterization, as the name suggests, includes applicable characterization tests for the cleaned modules and Solar PV Glass Coupon to verify the health of the coupons as well as to infer baseline data to compare the soiled modules' characterizations.

1. Test Module Characterization

The Angle of Incidence effect measurement for the cleaned modules was done. Then, the optical response of the Test modules was compared with the Sandia Polynomial to verify if the optical response of the Test modules was ideal. This clean optical response was compared with the soiled modules optical response as the soil density of the test modules varies.

The reflectance characterization accompanied the Angle of Incidence measurement for the cleaned modules. For each module, three sample spots were selected such that they represented the whole area of the test module while keeping ease of access in mind. The average of these three measurements was taken as the control measurement to compare the soil reflectance measurement.

2. Solar PV Glass Characterization

Two Solar PV glasses were used in this study. Transmittance through each of the glasses was measured using the Spectroradiometer after measuring the direct transmittance of the sun. This transmittance loss through the glass was compared to ensure the spectral loss properties were similar for both the glass pieces.

1.3.2.2.Soiled Modules Characterizations

Before the start of the experiment, a preliminary analysis was done to understand the soil collection rate dependence on the direction the modules were facing. The modules on trackers facing true-south and south-west were initially experimented, and it was found out that the modules facing south-west had higher and uniform soiling density when compared to the true-south facing modules. As expected the south-west wind is a major contributor to the soiling rate at our site in Mesa, Arizona. Therefore, the tracker was adjusted to face the south-west direction at 33° for the test duration to obtain a higher soiling rate and to maintain a uniform soiling layer. The modules were cleaned before setting the tracker in the south-west direction to naturally collect soil. However, the modules had to be cleaned again after a rain event in the due course of the experiment. The soiled characterization tests were performed weekly since the soil density varies. However, the transmittance and angle of incidence study were not performed on certain weeks when the irradiance was low or had a higher diffuse percentage.

1. Soil Sampling Module

The soil density of Soil Sampling Module on the two-axis tracker was measured for every round of Soiled Module Characterizations. This density measurement is the Soil Density (SD) for the corresponding soiled module characterizations. The whole module was divided into fixed sample areas (compounding three cells), and the soil density was calculated for a sample area in every round following ASU-PRL standard operating procedure (Appendix A) for measuring soil density using a lint roller, but four density measurements per module were not taken. A pre-weighed clean lint roller is used to

collect soil from the surface of the module in the sample area. The lint roller with soil is weighed and the soil density is measured using the following formula.

$$SD = \frac{(Weight_{Soil} - Weight_{clean})}{Area} \quad (8)$$

This soil density was considered as the soil density corresponding to the round. Mettler Toledo Analytical Balance (AG285, resolution 0.001 mg) was used to weigh lint rollers. For the purpose of this study, it is assumed that the soil density variation across the Soil sample module and across different test modules is very negligible.

Figure 9 Soil Sampling Modules

2. Test Module Characterization

In the case of soiled module characterizations, angle of incidence effect measurements and reflectance measurements were done for soiled modules. The measurements procedure is similar to the cleaned module characterizations. The reflectance measurements were taken at the exact same spots as the cleaned measurements were done. The reflectance measurements can be performed irrespective of the environmental conditions, but the angle of incidence measurements have certain requirements. Hence,

the angle of incidence effect measurements were not performed for the weeks when the conditions were unfavorable. However, reflectance measurements were performed for these weeks.

3. Solar PV Glass

For understanding the effect of soiling on transmittance, the irradiance spectrum was collected directly from the sun and then behind the cleaned and soiled Solar PV Glass. The cleaned glass was left outdoors with the soiled glass, but cleaned prior to each measurement. The spectrum was collected for three spots per glass and the average irradiance data was analyzed. All the measurements were performed with minimum delay to eliminate the effect of any possible spectral variation. All the measurements were done at 0° angle of incidence to avoid angle of incidence effects.

1.3.3. Angle Of Incidence Effect on PV Modules

The Angle of Incidence influence measurement is done following the Sandia National Laboratory Method.

1. Standard and Constant Irradiance: The global irradiance consists of some percentage of diffuse irradiance, even on clear days. To negate influence of diffuse irradiance, the Sandia method requires the experiment to be performed when the direct irradiance (irradiance measured by pyrheliometer) is 90% of the global irradiance (irradiance measured by pyranometer), i.e. the ratio should be greater than 0.85. To ensure that the irradiance variation is minimal, the experiment needs to be performed on clear days within a 20-minute period.

2. Standard and Constant Spectrum: Spectrum, like irradiance and temperature, effect the performance of the module. Therefore, spectral variation needs to be minimal during

the course of the angle of incidence effect experiment to avoid having to correct the performance for spectral variation. Therefore, ideally the measurements are performed around noon when the variation is negligible. However, considering the tracker limitation, the tests were performed between 13:00 and 14:00 MST, and the spectral variation for this test period can be considered negligible as well.

3. Temperature: The temperature of the module is one of the most significant factors in performance of the module. To avoid temperature influence, the temperature needs to be maintained constant. Nevertheless, this is not possible during the course of the experiment as the angle of incidence changes the irradiance, thereby changing temperatures. Therefore, the temperature of the modules was monitored to correct for temperature effect.

4. Data Points: The aim is to take as many data points as possible from angle 0° to 90° within the 20-minute period to maintain a high confidence level. The multicurve tracer takes about 2 sec per IV curve, and considering tracker constrain and angle of incidence measuring device constrain, 27 data points could possibly be collected. However, it was observed that beyond a 75° angle of incidence, ambient reflections effected the data. So, only a total of 23 data points were collected from 0° to 40° in incremental steps of 5°, and then in increments of 2.5° up to 75°.

1.3.4. Reflectance Measurement

The reflectance measurements used FieldSpec 4 Wide-Res spectroradiometer and Hi-Brite Contact Probe from ASD Inc. It uses user interface called RS^3 for control and data storage. The instrument measures relative reflectance with respect to a white reference. The following is a short description of the procedure. Please refer to Appendix B for a complete descriptive procedure.

1. Warm Up: Only 15 minutes of warm up is required for reflectance measurements.

2. Optimization: Optimization is the process of setting the instrument's electronics to optimally process the incoming signal. This means that the digitalization of the light signal is within a range of values that provide good signal-to-noise performance and does not allow the instrument to saturate at the current light levels.

The instrument must be re-optimized if:

- Atmospheric conditions change.
- The light source changes.
- The instrument is in the process of warming up and the response changes substantially.
- The instrument is saturating.

Outdoor conditions can change rapidly or slowly. It all depends on clouds, wind (affecting temperature), instrument warm-up time, etc. The instrument needs to be optimized to the ambient condition before the reflectance measurements. This is done through the optimize option in the software.

3. White reference: Spectralon panel (a calibrated white reference (WR)) that is attachable to the contact probe is used for white reference measurement. The instrument

needs to collect white reference every 10 to 15 minutes when indoors, or with an accessory light source, as in this case.

4. Measurement: The contact probe is placed perpendicularly on the coupon surface, and then spectrum is collected and saved using the software. The default average values were used.

5. Post Processing: The data files saved as .asd files were converted to .txt files using ViewSpecPro software provided by the manufacture.

1.3.5. Transmittance Measurement

The reflectance measurements used FieldSpec 4 Wide-Res spectroradiometer with a reflective cosine receptor (RCR) which enables hemispherical absolute energy measurements. The following is a short description of the procedure. Please refer to Appendix B for a complete descriptive procedure.

1. Warm Up: An hour of warm up time is recommended for radiometric measurements.

2. Optimization: Since the measurements are outdoors for transmittance, the optimization needs to be done with changing outdoor conditions. Optimization was done by pointing the RCR to the brightest source of light. Then 'RAD' is pressed to collect radiometric measurements.

3. Measurement: The RCR placed pointing at the light source and the spectrum is collected and saved using the software. In the current scenario, the light is the sun. The default average values were used.

4. Post Processing: The data files saved as .asd files were converted to .txt files using ViewSpecPro software provided by the manufacture.

1.4. RESULTS AND DISCUSSIONS

In this study, various characterization techniques have been used to understand the soiling losses experienced by modules of five different technologies as they naturally gather dust. The characterization tests were performed to identify soiling influence on AOI effect, and transmittance and reflectance spectrum. The transmittance spectrum gives first order information on basic transmission loss, while measurement of relative optical response throws lights onto the accompanying Angle of Incidence related to soiling losses that are often not considered in the field measurements, but have a huge impact. The reflectance spectra gives insight into any losses that can be specific to certain wavelength bands, if any, due to soiling.

1.4.1. Effect of Soiling on Transmittance

The effect of soiling on transmittance was calculated by finding the difference between transmittance spectrum of cleaned and soiled glass at 0° AOI. Figure 10 gives the transmittance measurement for cleaned and soiled glass along with direct transmittance at a soil density of 0.869 g/m^2. Only four soil densities were considered in the transmittance study. The transmittance loss was measured between wavelengths of 400 nm and 1100 nm, considering this is the response region of test modules as shown in Figure 11.

$$\text{Transmittance loss}_{\text{soiling}}\% = TL_{Soiled\ Glass}\% - TL_{Soiled\ Glass}\% \quad (9)$$

$$TL_{Glass}\% = \frac{Irradiance_{Direct} - Irradiance_{glass}}{Irradiance_{Direct}} * 100 \quad (10)$$

Where Irradiance is the cumulative sum of irradiance for 400 nm – 1100 nm band.

For Mesa soil types, soiling loss at 0° AOI increases by 0.0544% for 1g/m^2 soil density based on the equation in Fig. 11 and maximum measured loss was 4.93% at 0.869 g/m$^{2.}$ This includes reflectance and transmittance losses at 0° AOI.

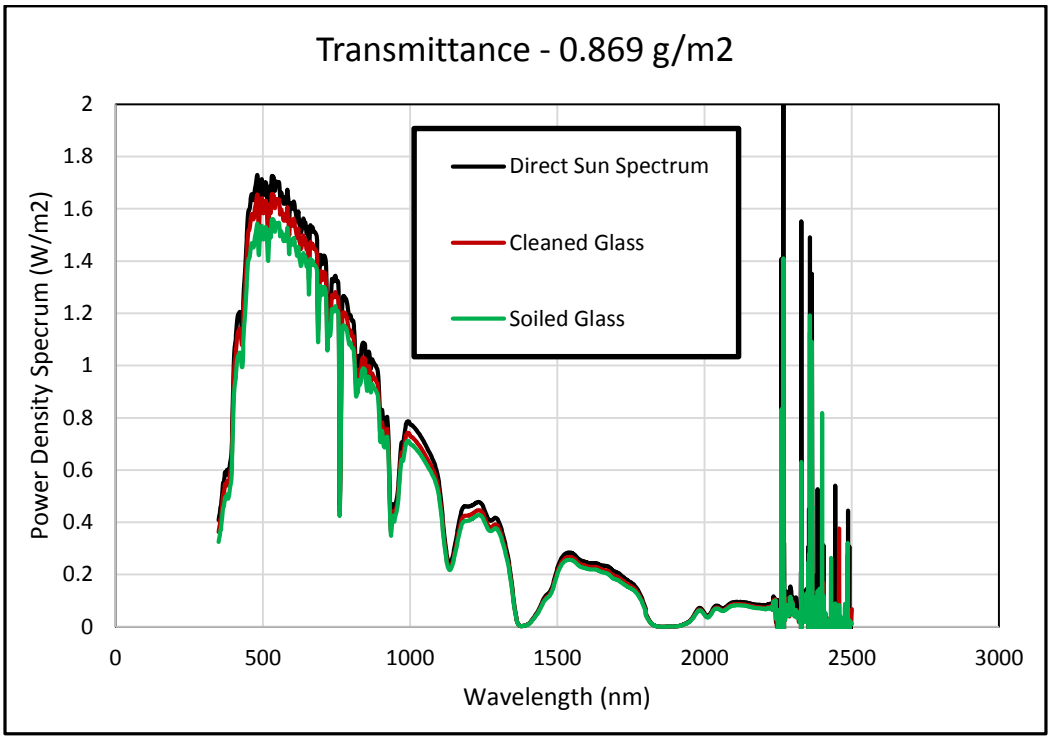

Figure 10 Transmittance Measurement for 0.869 g/m^2

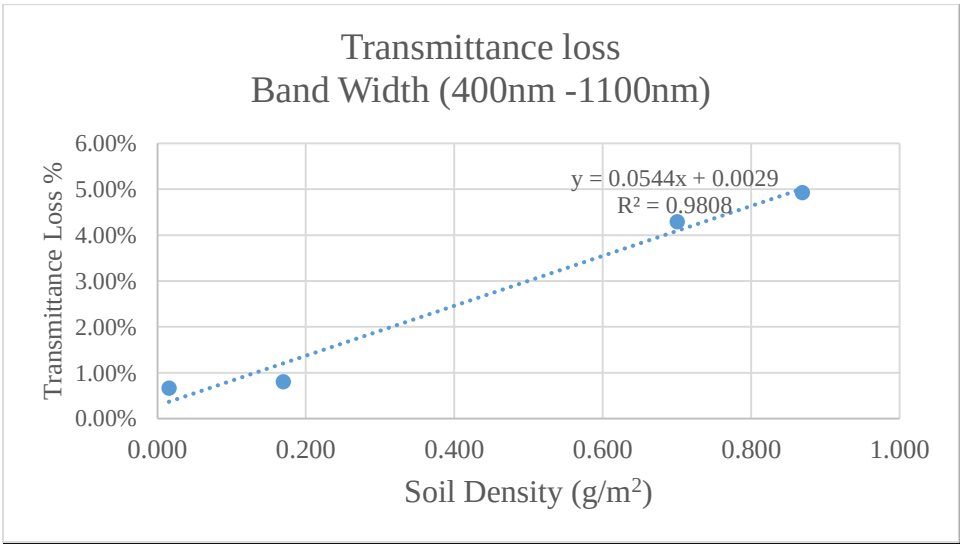

Figure 11 Transmittance loss Vs Soil Density

1.4.2. Influence of soiling on Reflectance

To understand the spectral influence of soiling directly from the field modules instead of the usage of glass, reflectance spectrum has been collected for all modules for the wavelengths between 350 nm to 2500 nm at three different spots. The average reflectance of cleaned modules was compared with the average reflectance of soiled modules for various soil densities. Fig. 12 gives the reflectance spectrum for all the technologies for cleaned modules.

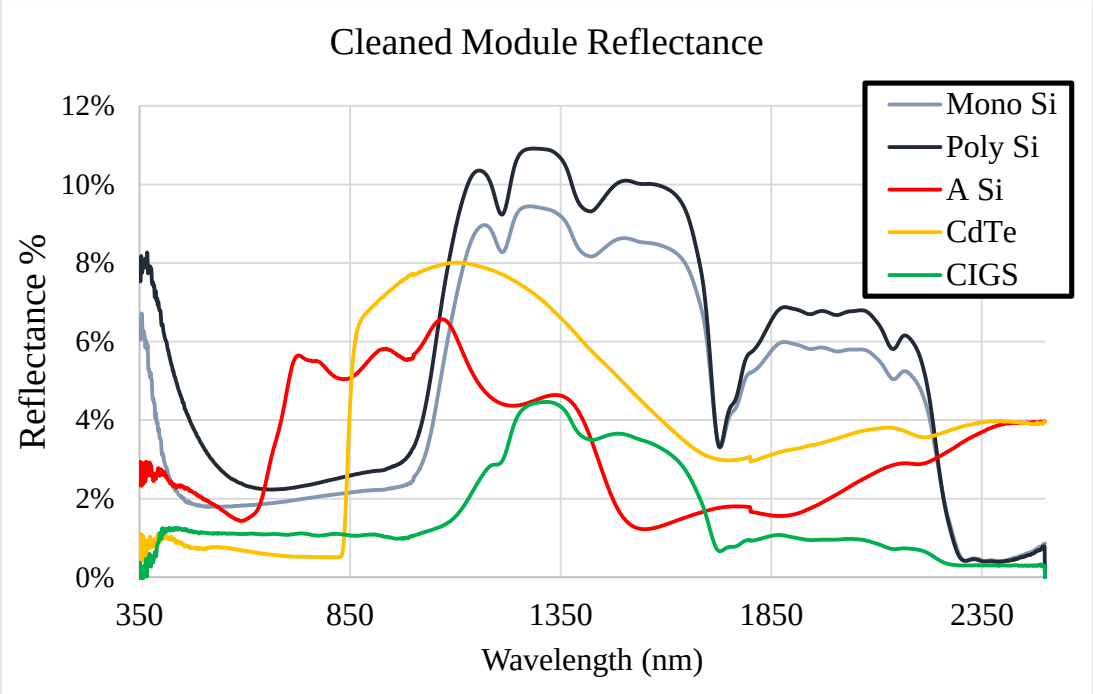

Figure 12 Cleaned module reflectance for all module technologies

It can be observed that technologies of similar band gaps exhibit similar reflectance spectra like the crystalline silicon technologies and CIGS. All the technologies show a valley in the corresponding absorption regions. An additional valley/dip was observed at 1700nm in crystalline Si technologies and CIGS, which is not

observed in thin film technologies of CdTe and a Si. This valley/dip is due to the presence of EVA. Even though EVA is present in all technologies, thin film technologies of CdTe and a Si have transparent conducting oxide (TCO) before the cell and EVA behind the cell. In crystalline Si technologies and CIGS, EVA is before the cell therefore, the absorption peak can be observed at about 1700 nm for these technologies.

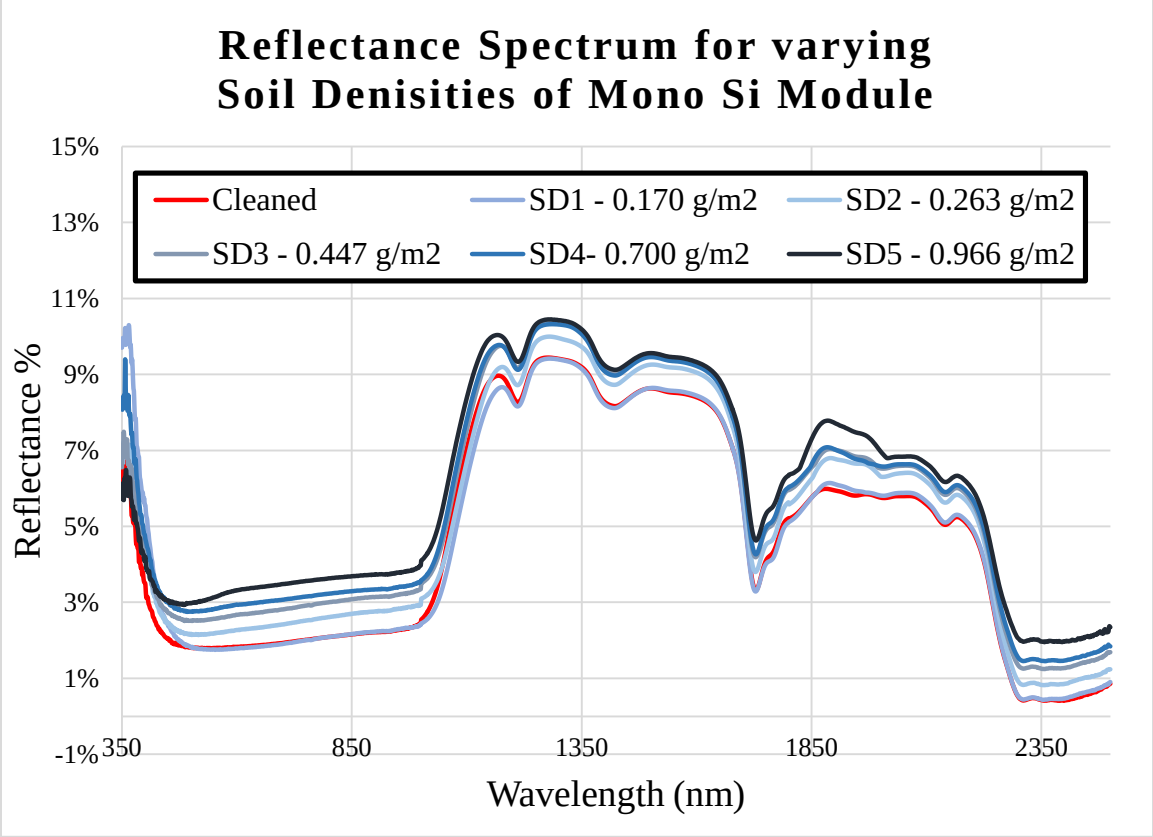

Figure 13 Reflectance Spectrum for different soil densities for Mono Si module.

The comparison includes five soiling densities ranging from 0.170 g/m^2 to 0.966 g/m^2. The following Fig. 13 gives the reflectance spectrum as soil density changes for Monocrystalline silicon. Refer to the Appendix C for the spectrum for all technologies.

The reflectance spectrum for any technology can be divided into two bands – the visible region and near IR region. The reflectance spectrum in the visible region corresponds to reflectance losses due to soiling, and the IR region spectrum gives

information of soil moisture and other soil properties. It was observed that in the visible region for all technologies, with the exception of amorphous silicon, there are uniform losses for all wavelengths. However, even for amorphous silicon, which can absorb up to 700 nm, there are uniform losses for this region as well. For a better understanding of soiling effect on reflectance, delta, which is the difference between cleaned and soiled reflectance, has been plotted across wavelength. Fig. 14 and Fig. 15 are the delta plots for Mono Si and CdTe.

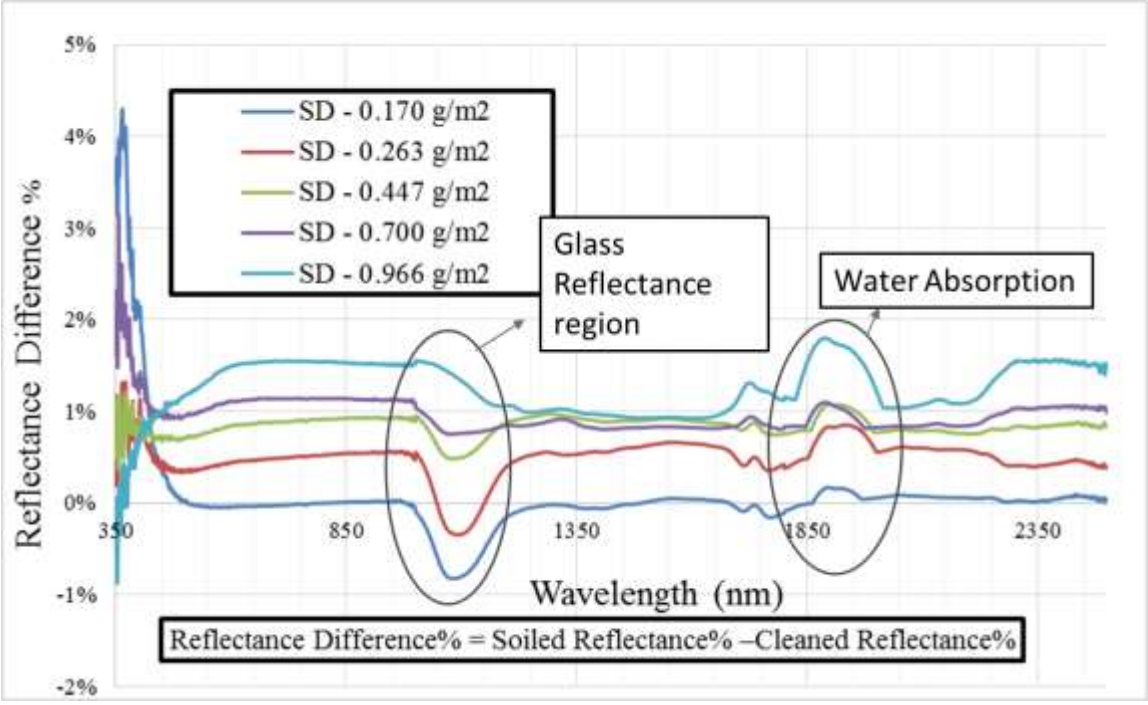

Figure 14 Delta Plot for Mono Si at different soil densities

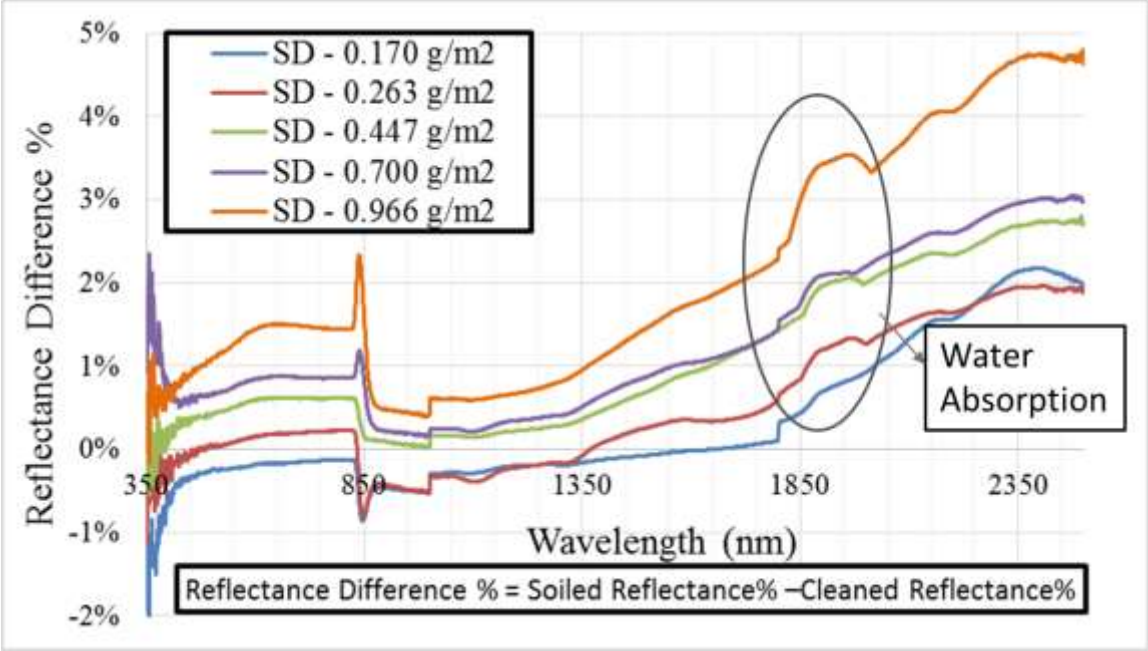

Figure 15 Delta Plot for CdTe at different soil densities

Delta plots for all technologies have been plotted (Appendix C), and water absorption peaks have been found for all technologies at around 1900 nm. The absorption peaks increased with soil density, which is due to higher moisture content in the soil. The height of this peak was found to be higher for crystalline Si technologies over thin films for same soil density, indicating higher moisture content in the surface soil of Crystalline Si technologies. This could be attributed to the glass type. Crystalline Si technologies use tempered glass while thin film technologies use annealed glass. The peaks and valleys pattern in the tempered glass could allow accumulation of thicker layer of soil in the valleys leading to un-vaporized trapped moisture in the soil and that could be the reason behind higher moisture content in crystalline Si modules.

Reflectance soil loss can be calculated as the difference between cleaned and soiled reflectance at a particular spot. Soiling density can be estimated from reflectance soil loss. The average reflectance soil loss over 600-700 nm wavelength band can used to

estimate soil density for all the technologies using the equations given in Table 5. The reflectance loss has been used, instead of measured reflectance of soiled modules, to account for, if any, localized variations in reflectance spectrum of cleaned modules.

Table 2 Soil Density estimation using average reflectance loss over 600 – 700 nm band.

Technology	Equation for Soil density estimation (in g/m^2) based on reflectance loss x = reflectance difference (Soiled reflectance% - Cleaned reflectance%)
Mono-Si	SD = 58.22x +0.055
Poly-Si	SD = 58.09x -0.046
a-Si	SD = 68.50x +0.262
CdTe	SD = 53.47x +0.196
CIGS	SD = 58.53x +0.052

1.4.3. Effect of Angle of Incidence on performance of Soiled Module

The relative optical response (f_2(AOI)) for all the cleaned modules was calculated using Sandia's procedure and model. This data for all technologies is compared with a "generic" polynomial model of Sandia, and was found to agree as shown in Figure 16. This was done to verify if the relative optical response of all the test glass superstrate modules is in congruence with the draft standard that states that: "For modules with a flat uncoated front glass plate made of standard solar glass, the relative light transmission into the module is primarily influenced by the first glass-air interface".[7]

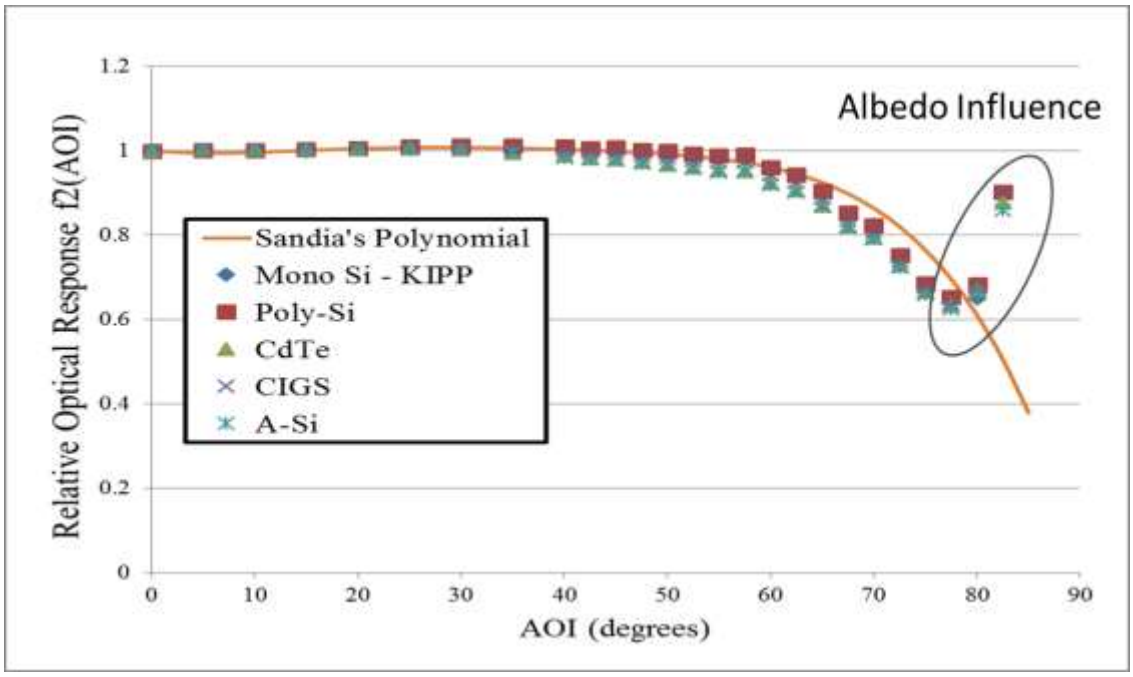

Figure 16 Relative optical response for cleaned modules of five technologies.

The thin films use annealed glass (smooth glass surface) whereas crystalline Si technologies use tempered glass (slightly rough glass surface). This influences the relative optical response curve, resulting in small variations between tempered glass and annealed glass. The experiment was conducted for all the modules over a time-period of two months (Oct – Nov), i.e. the second dry period of the year, as modules have a natural soil build up. The relative optical response of modules of five different technologies was calculated for five soiling densities as listed in Table 3.

Table 3 Soil Density for five rounds of AOI measurements

S. No	Date	Soil Density (g/m2)
SD1	1-Oct	0.016
SD2	22-Oct	0.263
SD3	3-Nov	0.345
SD4	11-Nov	0.447
SD5	25-Nov	0.649

For each round, the Relative Optical Response f_2(AOI) verses AOI curve was plotted for all the technologies, and it was observed that the response is similar to all technologies for all soil densities.

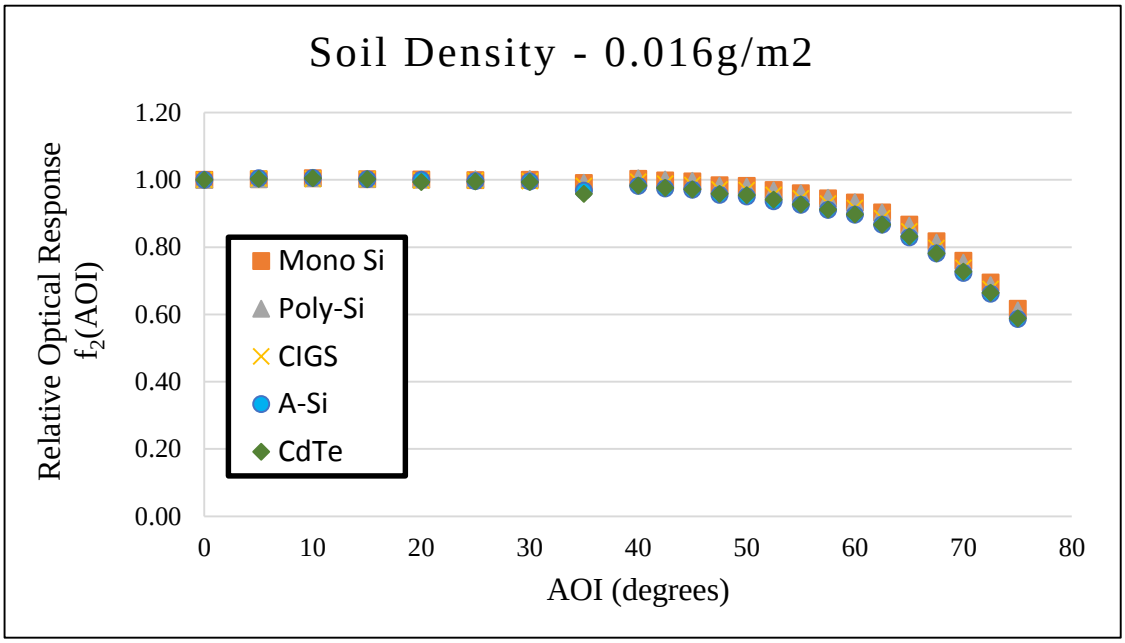

Figure 17 Relative optical response for modules of five technologies when soil density is 0.016g/m^2.

Figure 17 and Figure 18 are the relative optical response plots for the least and highest soil densities that have been observed during the study period. This indicates that in the case of any field module, the most dominant interface changes from air/glass interface to air/soil/glass interface due to soiling and the variation in f_2(AOI) is dependent on soil type and density. Moreover, the relative optical response is constant for all modules at a particular soil density, but the response itself varies with change in soil density as shown in Figure 17 and Figure 18. As the effect of soil is independent of module technology, the plots for Mono Si module have been considered for further analysis to understand the effect of soil density on AOI losses as shown in Fig. 19.

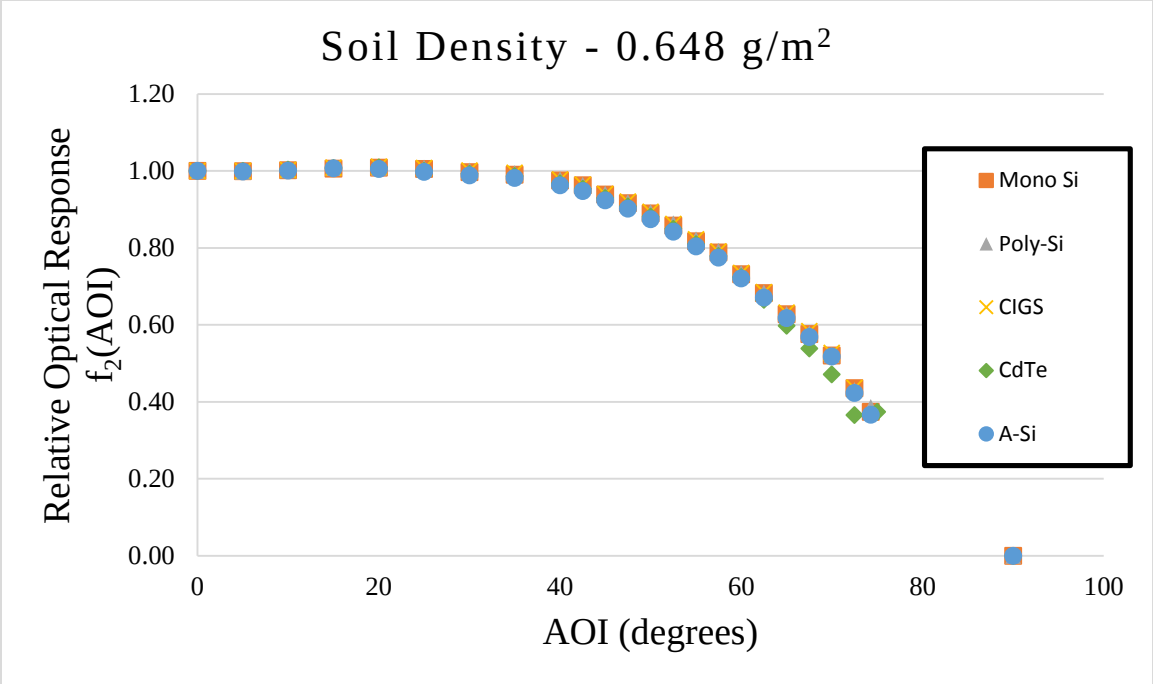

Figure 18 Relative optical response for modules of five technologies when soil density is 0.648g/m^2.

Figure 19 illustrates that as the soil density increases, the drop in the f_2(AOI) beyond critical angle also increases, indicating that the reflective losses increase at higher AOI due to soiling. In other words, the power or current loss between clean and soiled modules would be much higher at a greater AOI than at a lower AOI, leading to excessive energy production loss from soiled modules on cloudy days, early morning hours and late afternoon hours.

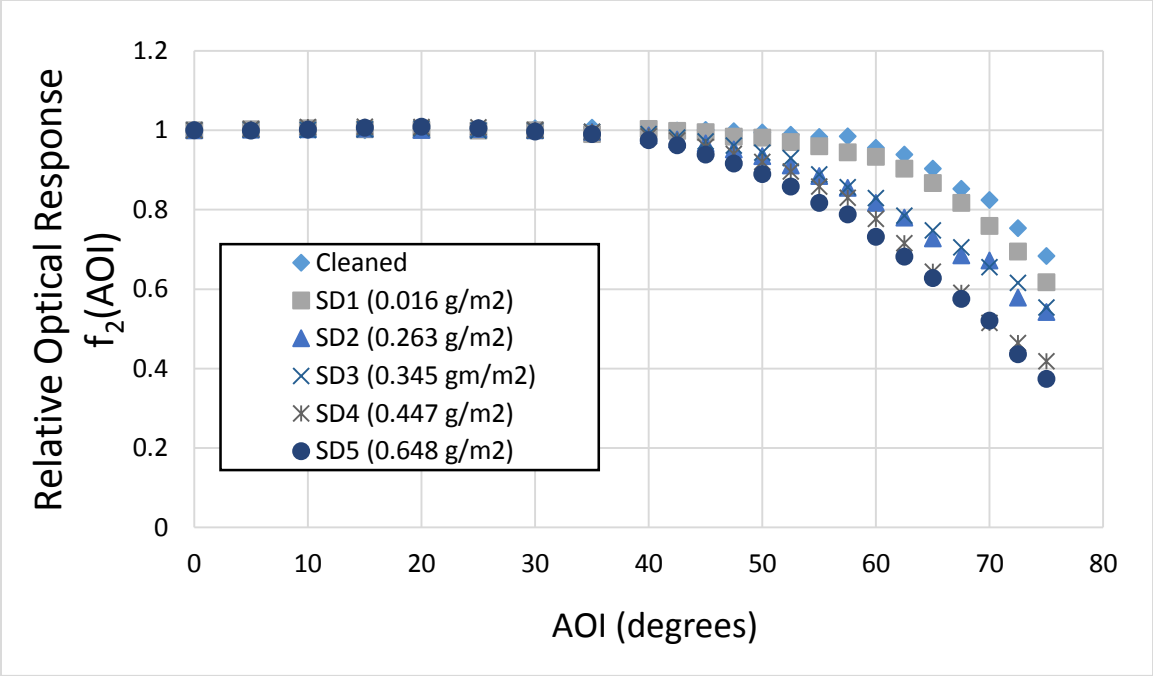

Figure 19 Relative optical response for Mono Si as soil density varies.

Critical Angle Calculation

The critical angle is defined as the angle above which there is a loss of 3% or above as compared to the 0° AOI [8]. The critical angle for the cleaned module (i.e. 0 g/m^2 soil density) is 57^o, but, as shown in Figure 20, this critical angle drops as the soiling density increases and reaches a near constant minimum of 40^o beyond 0.2 g/m^2 for up to the maximum measured soiling density of 0.648 g/m^2. Due to a rain event in the late fall season of 2014, the study was not continued beyond the soiling density of 0.648 g/m^2. Based on these observations, it can be stated that the critical angle shifts from 57^o for the clean air/glass interface to 40^o for the naturally developed air/soil/glass interface in Mesa, Arizona for the fall season. This information could be particularly important in case of fixed tilt systems which produce a larger portion of energy at higher AOI.

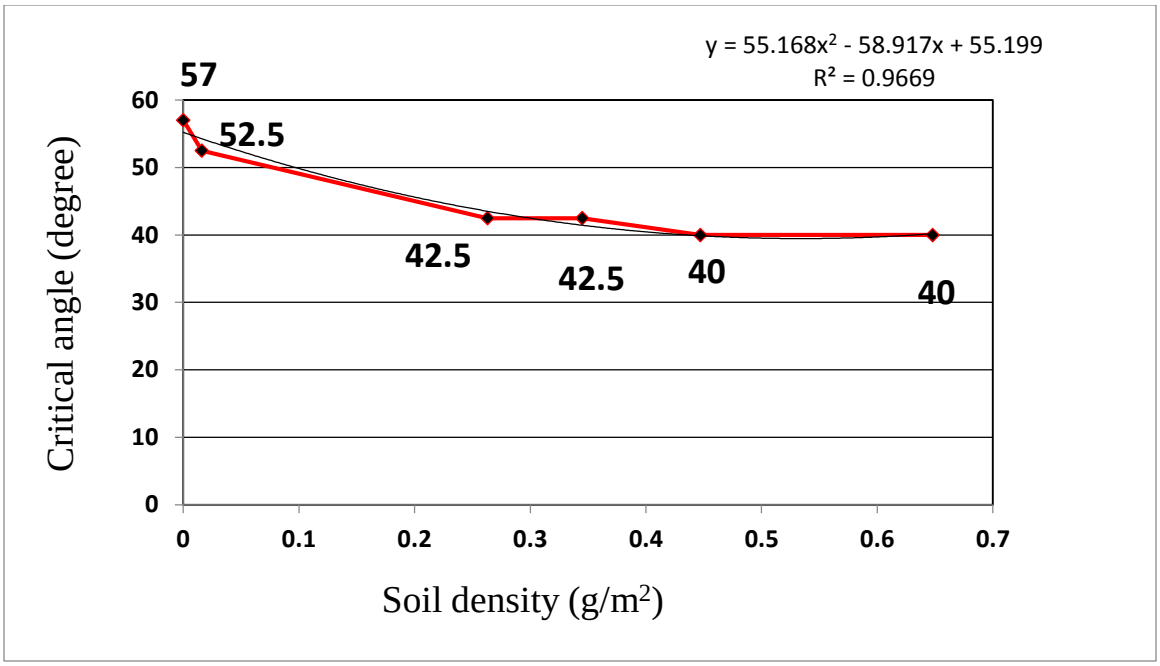

Figure 20 Critical angle Vs. Soil Density

The empirical polynomial equations providing the relationship between soiling density and f_2(AOI) is provided in Table 2. Only Mono-Si technology equations are shown in this table, as other technologies have been found to have almost identical equations.

Table 4 Summary of observations from AOI curve of soiled PV modules

Rounds	Soil Density (g/m^2)	Critical angle (degree)	Empirical Formula ($f_2(AOI)$) (Formulated using Excel Spreadsheet)
1	0.016	52.5	$f_2(AOI) = -5E\text{-}06(AOI)^3 + 0.0004(AOI)^2 - 0.009(AOI) + 1.0357$
2	0.263	42.5	$f_2(AOI) = -3E\text{-}06(AOI)^3 + 0.0002(AOI)^2 - 0.0022(AOI) + 1.0067$
3	0.345	42.5	$f_2(AOI) = -3E\text{-}06(AOI)^3 + 0.0002(AOI)^2 - 0.0028(AOI) + 1.0087$
4	0.447	40	$f_2(AOI)\ -1E\text{-}06(AOI)^3 - 5E\text{-}05(AOI)^2 + 0.0042(AOI) + 0.9777$
5	0.648	40	$f_2(AOI) = -1E\text{-}06(AOI)^3 - 9E\text{-}05(AOI)^2 + 0.0048(AOI) + 0.9752$

1.4.4. Modelling of Soiling Losses Due To Effect of Angle Of Incidence

All the modules were cleaned after a rain event on the 20th of October, and the experiment was performed on the 22nd of October for soil density of 0.263 g/m^2 that has been accumulated over a period of two days. The corresponding relative optical response curve is given in Fig. 21. Considering the soil density as uniform soil density throughout the year, annual soiling losses due to AOI effects were calculated for different regions. Weather data from Solar Anywhere was used for Phoenix while PVSyst weather data based on MeteoNorm was used for other locations.

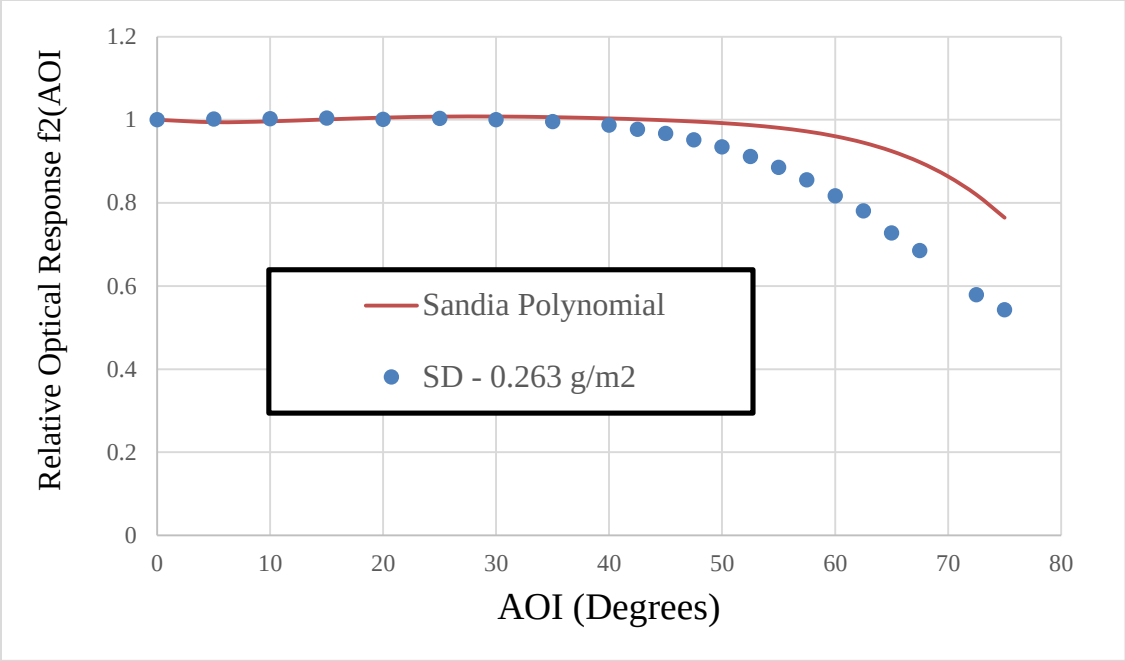

Figure 21 Relative Optical Response for cleaned and soiled module of SD 0.263 g/m^2

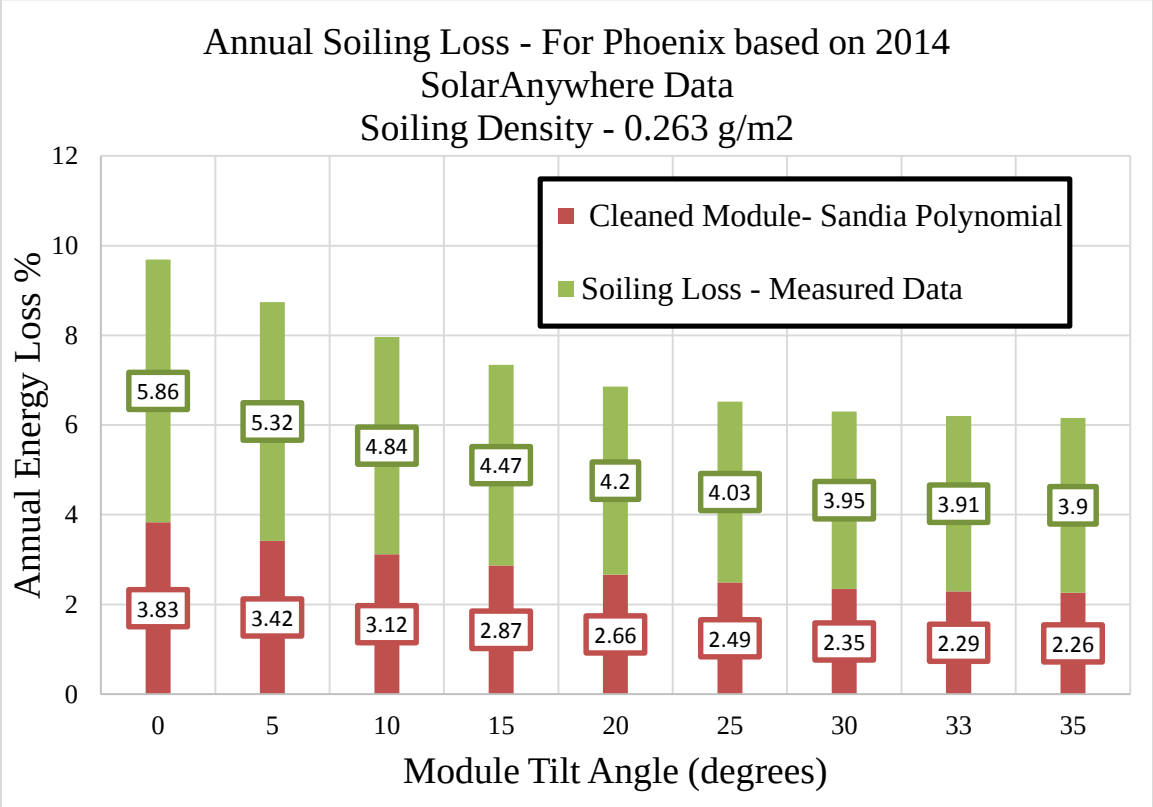

Figure 22 AOI related soiling Annual Energy losses - Phoenix

The angle of incidence related losses for a particular tilt for a cleaned module have been estimated using Sandia's polynomial with PVsyst. Similarly, the angle of incidence related losses for soiling modules has been estimated to be 0.263 g/m^2 AOI polynomial with PVsyst. The calculation has been done for all tilt angles from 0^o to 35^o in increments of 5^o, and for the latitude tilt of the location. The difference between two losses, i.e. AOI related Soiling losses, ranges from a minimum of 3.9% for 35° to a maximum of 5.86% at 0^o for Phoenix as shown in Figure 18. The estimation was done using SolarAnywhere weather data for the year 2014.

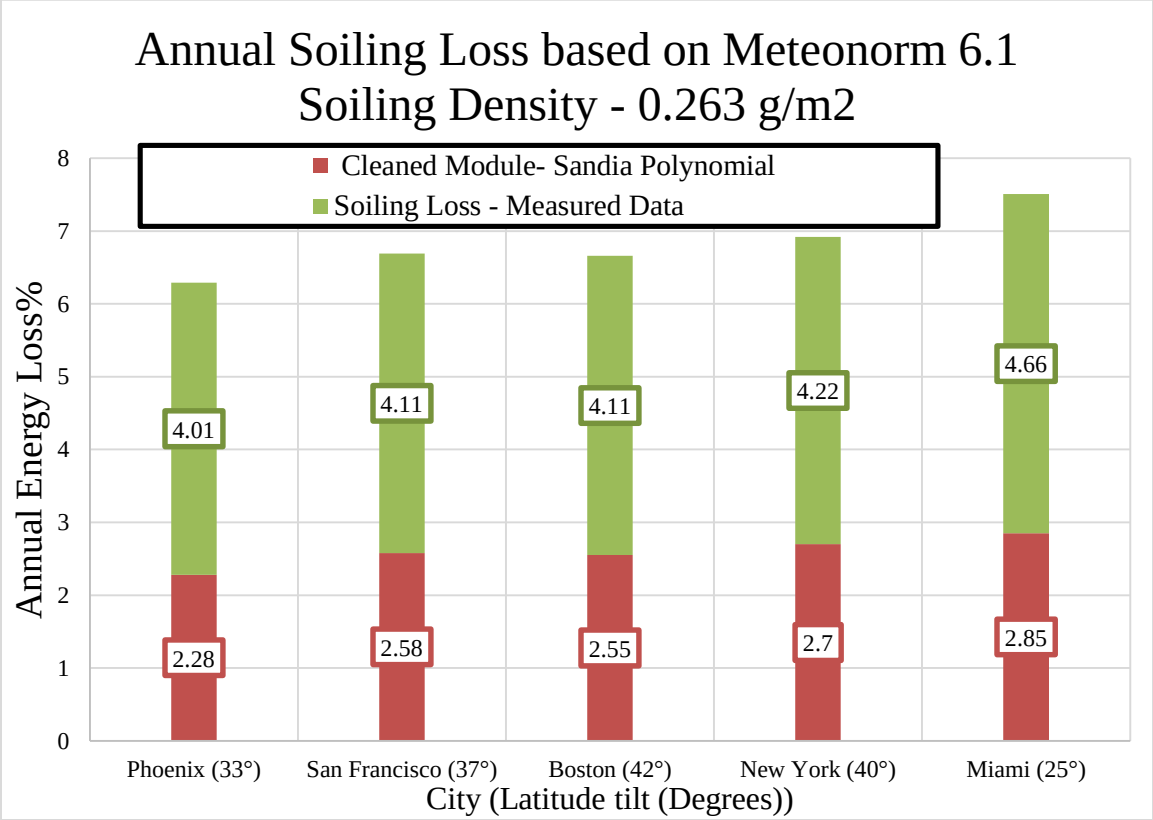

Figure 23 AOI related annual energy soiling losses for different locations using measured data

Similar analysis was done for other locations like New York, San Francisco, Boston, and Miami, along with Phoenix, as given in Figure 23 based on MeteoNorm

weather data. It was observed that the losses were higher in these locations when modules are mounted at corresponding latitude tilt as compared to Phoenix. This could be attributed to the presence of a larger percentage of diffuse irradiance in these locations as compared to Phoenix. However, it is to be noted that the relative optical response could differ based on the soil type of the location, and the soil density is not constant throughout the year. The soil density of 0.263 g/m^2 was observed after two days of field exposure in Mesa. Therefore, while these values can be considered as the minimum expected soiling losses, actual soiling losses are completely dependent on the location.

1.5. CONCLUSION

- If there is an identical soil density on the PV modules, then the relative optical response at different AOI, i.e. f_2(AOI), will be nearly identical, irrespective of the PV technology type, with air/soil/glass becoming the most dominant interface.
- The power or current loss between clean and soiled modules would be much higher at a higher AOI than at a lower AOI leading to excessive energy production loss of soiled modules on cloudy sites or days, early morning hours and late afternoon hours.
- Based on the results obtained in this study, it can be stated that the critical angle shifts from 57^o for the clean air/glass interface to 40^o (0.648 g/m^2) for the naturally developed air/soil/glass interface in Mesa, Arizona for the fall season.
- Using an average reflectance measurement between 600-700 nm bandwidth, the soil density of the module can be estimated. By using the empirical formula presented in this work, f_2(AOI) values for any AOI, as well as transmission losses, can be estimated if the soil density is known/measured.
- If the soil density is known, the angle of incidence related losses for the whole year can be modelled using PVSyst for Mesa soil type.

The indoor and outdoor soiling studies were jointly performed by two Masters students, Sravanthi Boppana and Vidyashree Rajasekar. This thesis presents the outdoor soiling study, whereas, the other thesis presents the indoor soiling study. Major conclusions resulting from this study are as follows:

- Gravity-assisted and laser-guided approach of spraying soil on to coupons helps in improving the soil uniformity pattern. Total area of the test coupon for soil application can be further increased by increasing the distance between the module and spray gun.
- Mini-modules can be used to check uniformity by measuring I-V curves, whereas, for characterization tests, single-cell coupons are more favorable.
- With change in properties of a cell, backsheet/encapsulant over time can be determined by carrying out reflectance measurements on the cell and glass/EVA/backsheet respectively (white area).
- Particle size plays an important role in reflectance measurements. The smaller the particle size, the higher the reflectance scattering. Reflectance/QE can be used as a direct measure of soil density. The correlation plot between soil density (g/m^2), reflectance loss (%) and QE loss (%) varies linearly.

PART 2: STATISTICAL RISK ANALYSIS

FOR PHOTOVOLTAIC POWER PLANTS

2.1. INTRODUCTION

2.1.1. Background

Photovoltaic modules are typically warrantied to have a minimum of 20 years of lifetime use with less than 1% degradation per year. However, various field failures or degradation modes that can result in shorter lifetime and/or lesser performance of the modules. The lifetime of PV modules is typically dictated by the degradation rates rather than failure rates, and the multiple failure modes over time could have a cumulative influence on the degradation rates of the PV modules [9]. Therefore, by using the failure modes and degradations modes as indicators, one can attempt to predict the value of a power plant. Studies have been performed at ASU- PRL to identify the most-dominant failure modes for hot-dry climatic conditions of Arizona [11-13]. Sanjay et al. used the statistical tool of Failure Mode, Effect, and Criticality Analysis (FMECA) technique to identify the most dominant failure mode for PV industry [13].

This study attempts to identify the reliability and durability issues for a site in Cold-Dry climatic conditions of New York using non-destructive tools like IV characterization, diode check, etc. along with visual inspection of all the modules of the plant. The count and performance data obtained from these techniques is further used to carry out statistical analysis of FMECA to understand the failure modes for this particular climatic condition. The FMECA technique is a site-specific approach that used Risk Priority Number (RPN) for ranking failure modes. This study tries to differentiate RPN into safety RPN and degradation RPN to identify the most influential mode in terms performance.

2.1.2. Statement of Problem

Different environmental conditions contribute to different field stress conditions. It is important to identify the most prominent stresses for a particular climatic condition in risk analysis criteria as a step towards risk mitigation by manufacturers, and towards selection of climate-resilient module design by project developers. This would help in engineering solutions to mitigate these problems as preventive measures. Plant owners can use the FMECA/RPN technique to determine the state of health of the power plant and then prioritize and assign resources depending on RPN. The eventual goal of a RPN study would be to classify power plants into classes based on their Safety RPN and Degradation RPN as shown in Fig. 24. The class boundaries would be climate specific.

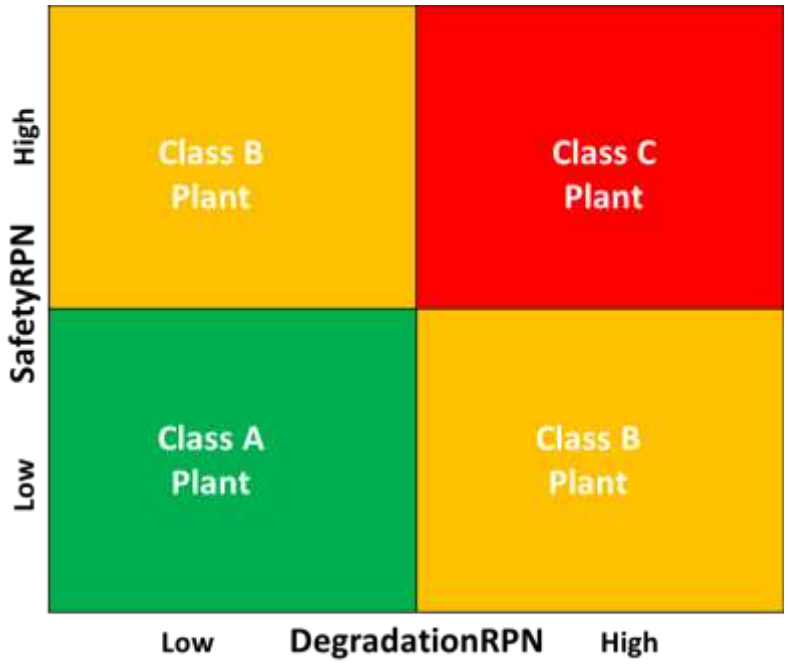

Figure 24 Grading PV Power Plant- Conceptual approach

In this study, field measurements were performed to identify failure and degradation modes and FMECA analysis as done based on this data. This study aims at

identifying the prominent failure mode for field modules of Cold-Dry climatic conditions and understand the safety, reliability and durability failures observed in the field for cold-dry climatic condition by comparing two power plants of same manufacturer, same climate zone and similar age.

2.2. LITERATURE REVIEW

2.2.1. Failure Modes and Degradation Modes

In the PV Industry, the terms reliability and durability are used extensively in the context of the lifetime of PV. It is important to understand the meaning of these terms in order to comprehend the reliability failures and durability failures. If the PV modules are removed (or replaced) from the field before the warranty period expires due to any type of failure, including power drop beyond warranty limit, then those failures may be called a reliability failure. If the performance of PV modules degrades, but still meets the warranty requirements, then those losses may be classified as soft losses or degradative losses. Durability losses may be defined as degradative losses that meet the warranty requirements, and the reliability failures may be defined as catastrophic and wear-out failures that do not meet the warranty requirements [9]

This knowledge is essential to identify and differentiate failure modes and degradation modes. The following table from SolarABC report 'Accelerated Lifetime Testing of Photovoltaic Modules' by *TamizhMani and Kuitche* [9] gives insight into various failure modes and degradation modes. The degradation modes are listed separately from failure modes, but most of the failure modes are also caused by the slow degradation modes, which could later become severe, leading to failure modes.

Failures and Degradation Modes of PV Modules

Failure Modes (Leading to immediate warranty returns)	**Degradation Modes** (Leading to power degradation warranty limit)
	
• Broken interconnects (leading to arcing, backskin burns, or glass shattering or power loss higher than warranty limit) • Solder bond failure (leading to backskin burns or glass shattering) • Severe corrosion (leading to backskin burns or power loss higher than warranty limit) • Chipped cells (leading to hotspots or power loss higher than warranty level) • Encapsulant delamination (leading to power loss higher than warranty level) • Broken glass (leading to safety issue) • Hotspots (leading to backskin burning and safety issue or power loss higher than warranty limit) • Ground faults (leading to safety issue or power loss higher than warranty limit) • Junction box failures (arcing or ground faults) • Connector failures (leading to safety issue) • Structural failures (leading to safety issue) • Bypass diode failures (leading to safety issue due to hot spot or power loss higher than warranty limit due to string loss)	• Gradual cracking of interconnects (leading to power degradation) • Gradual solder bond failure (leading to power degradation) • Slow corrosion (leading to metallization discoloration and power degradation) • Gradual cracking of cells (leading to power degradation) • Gradual encapsulant discoloration (leading to power degradation) • Gradual (photo)electrochemical degradation of semiconducting and/or metallic materials (potential induced degradation leading to power degradation) • Gradual backsheet warping (leading to power degradation) • Gradual increase of module mismatch (leading to power degradation) • Strongly adhering and gradual hardening of soil layer on superstrate (leading to slow cumulative/permanent increase in annual power degradation) or weakly adhering and rain/wind cleaning of soil layer (leading to fixed/temporary annual degradation due to non-cumulative reversible annual rain effect)

Modes and Mechanisms

The sequence of failure flow is a failure cause triggers a failure mechanism. A failure mechanism causes a failure mode and a failure mode results in a failure effect. The effect defines whether the mode is a failure mode or degradation mode. Furthermore, the relation is not one to one. In other words, a failure mechanism can lead to multiple

failure modes, etc. The following table lists a few modes that are relevant to the current study [9 ,14].

Table 5 Failure/Degradation modes and mechanisms

Failure mode	Failure Cause	Failure Effect	Failure mechanism
Encapsulant delamination	UV light; humidity; contamination from the material; tempering process caused by stress and weakened adhesion	Power degradation; optical decoupling of materials; reverse-bias heating; transmission loss	Photothermal Reaction Electro chemical reacation
Interconnect discoloursation	Moisture Ingress; High ambient temperature along with humidity	Increase in series resistance and decrease in power	Chemical corrosion
Backsheet Delamination	Poor adhesion between encapsulant and backsheet; Moisture ingress through backsheet	Ground Fault under wet conditions	Chemical reaction weakening interface bonds
By-pass Diode Failure	Thermal expansion and contraction; insufficient diode rating; Insufficient heat dissipation in Junction box	Open circuit failure of bypass diode(Possibly, no change in output) but suseptable to hot spot etc.; Short circuit failure leads to loss of power	Thermal fatigue
Encapsulant Browning	UV exposure at high operation temperature; Higher UV concentration; Inappropriate additives	Transmission Loss; Reduced power/current without fill factor effect or warranty limit;	Photothermal reaction(in presence of UV and higher module temperature)

		Cosmetic/Visual change	
Broken Glass	Due external factors like flying pebbles, etc. Hotspots or arcs; Support structure failure, etc.	Ground Fault and drop in power.	Thermo-mechanical fatigue

2.2.2. FMECA Technique

The IEC 60812 standard defined the failure mode and effect analysis (FMEA) as a systematic procedure for the analysis to identify the potential failure modes, and their causes and effects on system performance [15]. FMECA extends FMEA with an addition of detailed quantitative analysis of criticality of failure modes (severity). Ideally, FMECA is conducted in the product design or process development stage, or after a quality function deployment to a product, but conducting it on fielded systems/products also yields benefits. FMEA/FMECA analysis allows a good understanding of the behavior of a component of a system, as it determines the effect of each failure mode and its causes. The study of criticality quantifies the effect of each failure mode so that the effect of these failures could be minimized prior to action [15].

The process of FMECA analysis consists of preparing a FMECA worksheet to include potential failure modes, their causes or mechanisms, and identifying a rating guideline. This study uses Risk Priority Number as a rating guideline.

Risk Priority Number

This follows the IEC 60812 2006-01 Standard [13] as an approach to quantify criticality of a failure mode. The risk priority number can be calculated as follows.

$$RPN = S * O * D$$

Where S stands for Severity;

O for Occurrence;

D for Detection.

Severity(S) is an estimate of how strongly a failure mode will effect a system or the user. It is a measure of criticality of a failure mode and a non-dimensional number. Occurrence (O) is the probability of occurrence of a failure mode for a predetermined or stated time period. It may be defined as a ranking number rather than the actual probability measure. Occurrence ratings are based on a cumulative number of module failures per thousand per year (CNF) which is a function of the total number of failures and the years of operation. For both severity as well as occurrence, higher ratings denote adverse effects. Detection (D) approximates the chance to identify and eliminate the failure before the system or user is affected. This number is ranked in reverse order from the severity or occurrence numbers: the higher the detection number, the less probable the detection is. This means that the low probability of detection will yield to higher RPN. The RPN number is the indicator of the criticality of the failure mode. A higher the RPN number signifies the adverse effect of the failure mode.

2.3. METHODOLOGY

For calculating RPN value for a power plant, the first step is to identify all the failure modes. This identification process includes visual inspection, IR Imaging, Diode check and IV curve measurement. The visual inspection was done following NREL checklist for Visual Inspection while IR Imaging was done using a Fluke IR Camera. Diode Check involves a line checker that helps identify if the diode has failed in open circuit or closed circuit condition. The IV curve measurement process is in two stages: String Level IV curve Measurement and Module Level IV curve measurement. For large power plants where the total number of modules are in the hundreds or thousands, it is not feasible to measure IV curves for each individual module. Therefore, in such cases, string level IV's were taken for all the modules, but module level IV's were taken for a selected sample size that would represent the whole power plant. The ideal case for a sample size selection would be 95% CL and 5% CI.

2.3.1. Determination of Occurrence

The Occurrence rating was assigned based on the IEC 60812:2006 Std. For this, a cumulative number of module failures per thousand per year (CNF) was computed based on the field data. The number of defects in the power plant, as well as its age, influences the CNF number. CNF number was computed using the following equation.

$$\frac{CNF}{1000} = \sum System\ (\%defects) * \frac{10}{\sum system\ (operating\ time)}$$

\

Table 6 Occurrence determination

Failure Mode Occurrence	Frequency CNF/1000	Ranking O
Remote: Failure is unlikely	<= 0.01 module per thousand per year	1
Low: Relatively few failures	0.1 module per thousand per year	2
	0.5 module per thousand per year	3
Moderate: Occasional failures	1 module per thousand per year	4
	2 module per thousand per year	5
	5 module per thousand per year	6
High: Repeated failures	10 module per thousand per year	7
	20 module per thousand per year	8
Very high: Failure is almost inevitable	50 module per thousand per year	9
	>= 100 module per thousand per year	10

2.3.2. Determination of Detection

The detectability criteria was designed based on ease of detection of a failure mode after the module is exposed to field conditions. The current study follows the procedure defined by Sanjay Shrestha *et al* [13]. When a failure has the most likelihood of detection, it is given a lesser detection number, while the least likelihood failure mode is given a higher number. The detection techniques include monitoring system detectability along with field techniques like visual inspection, IV measurement, etc. If a failure mode requires the use of advanced techniques that cannot be performed in the field for detection, then the failure mode is given the highest detection rating. The following is the detection table used in this study.

Table 7 Detection Determination

Ranking	Criteria: Likelihood	Detection
1	Monitoring System itself will detect the failure mode with warning 100%	Almost certain
2	Very high probability (most likely) of detection through visual inspection	Very high
3	50/50 probability (less likely) of detection through visual inspection	High
4	Very high probability (most likely) of detection using conventional handheld tool e.g. IR, Megger	Moderately high
5	50/50 probability (less likely) of detection using conventional handheld tool e.g. IR, Megger	Moderate
6	Very high probability (most likely) of detection using non-conventional handheld tool e.g. diode/line checker	Low
7	50/50 probability (less likely) of detection using non-conventional handheld tool e.g. diode/line checker	Very low
8	Very high probability (most likely) of detection using performance measurement equipment e.g. IV tracer	Extremely Low
9	50/50 probability (less likely) of detection using performance measurement equipment e.g. IV tracer	Remote
10	Detection impossible in the field	Absolutely uncertain

2.3.3. Determination of Severity

The severity of the failure mode can be considered the most significant of the three criteria as it encompasses the performance as well as safety information. The Severity number is dependent on the degradation rate per year of the module(s) with that particular defect. The degradation rate is calculated from the IV information as

$$Degradtion\ rate\ per\ year\ (Rd) = \frac{(Pmax\ drop * 100)}{Rated\ Pmax * age\ of\ operation}$$

where $\text{Pmax Drop} = \text{Rated Pmax} - \text{Current Measured Pmax}$

The typical warranty degradation rate of 1% per year is considered to be the moderate rate of degradation, hence given a severity of six. Degradation lower than 1% is

given a lower severity number ranging from one through five, while the higher severity numbers are given higher degradation rates up to a ranking of eight. Certainly, the higher severity rankings (8-10) justify safety concerns. The following is the table for severity determination.

Table 8 Severity Determination

Ranking	Severity Criteria	Severity
1	No effect, Rd < 0.3%	None
2	Insignificant, Rd approx. to 0.3%	Very minor
3	Minor Cosmetic defect, Rd < 0.5%	Minor
4	Cosmetic defect with Rd < 0.6%	Very low
5	Reduced performance, Rd < 0.8%	Low
6	Performance loss approx. to typical warranty limit, Rd approx. to 1%	Moderate
7	Significant degradation, Rd approx. to 1.5%	High
8	Remote safety concerns, Rd < 1% Or Rd > 1.5% with no safety concern	Hazardous with operable performance
9	Remote safety concerns, Rd < 2%	Hazardous with reduced level performance
10	Safety hazard, Catastrophic	Catastrophic

Ideally, the module degradation rate should be used with severity ratings so as to estimate the contribution of failure modes in the degradation of that particular module. However, in the case of large power plants, it might be not feasible to take IV curves of all the modules or even for the selected sample. Even if modules IVs were taken with an adequate sample size, not all the defects identified in visual inspection might be covered in the selected sample, as is the case of the current site. In this case, considering string

2.4. RESULTS AND DISCUSSION

In this study, a 19-year-old site from cold-dry climatic conditions of New York was analyzed using FMECA technique. Visual Inspection following NREL checklist, Diode check and IV characterizations were done as part of the field characterization techniques, which give the count data for occurrence ratings and performance data for severity ratings. The following table gives site specifications.

Table 9 Site description

Site Name and Location	Model JVA, New York.
Age	19 Years
Mounting and Frame structure	41° tilt Roof Top System with Framed modules
System Size	43.2 kW_{dc}
Inverter	36 kW_{ac} (Non – Operational for unknown time period, assumed to be for 4 years)
Number of modules	360

The system consisted of five arrays, with six strings in each array. Each string consisted of 12 modules summing up to 360 framed glass/polymer polycrystalline Si modules. One string in the system was found disconnected. The modules from this string were considered for safety failure analysis, but not in FMECA analysis. The system has a 36 kW_{ac} inverter that is non-operational and the duration for this failure is unknown. Assuming linear degradation and based on the string level degradation rate of Model J (refer Section 2.4.6. for a full description), it is estimated to have been non-operational for 4 years. Therefore, IR Imaging was not done as the system was in open circuit condition. The following table gives the module's specifications.

Table 10 Electrical Parameters of Module

Model	Pmax	Voc	Vmp	Isc	Imp
Model - JVA	120 W	42.1 V	33.7 V	3.87 A	3.56 A

2.4.1. Safety Failures

Visual Inspection and Diode Check were performed on all the modules of the power plant including the disconnected string. 6.1% of the total 360 modules (i.e. 24 modules) have safety concerns, as shown in Fig. 25. Of these 24 modules, five safety concerns were found in a single string that was disconnected from the array. Failed diodes have the possibility to cause backsheet burning, as there could be cell heat up. Modules that have circuit exposure from backsheet peels/scratches or have no frame grounding (ground faults) pose an electrical safety hazard to personnel. There was also one broken module that was found to pose a safety hazard due to not only the electrical hazard it possesses, but also due to the broken glass on the front surface of the module.

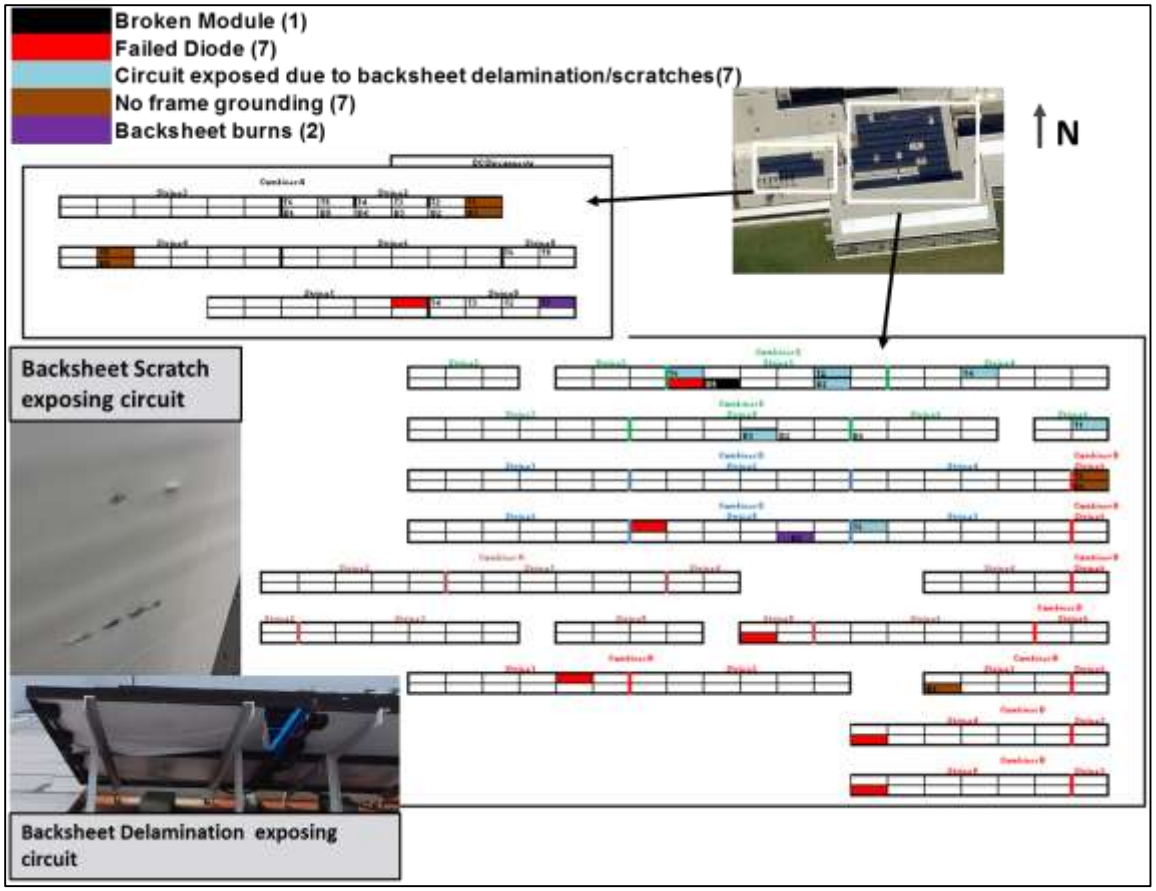

Figure 25 Safety failure

2.4.2. Degradation Rate

Of the 30 strings in the power plant, string level IVs were taken for 29 strings. The one disconnected string is not included in the analysis along with the safety concerns. The average string-level degradation was determined to be 0.6%/year, with 27 strings (93%) of the total 29 strings meeting the 1.0% degradation rate typically given by module manufactures. The following Fig. 26 gives the histogram of string level degradation rates for Model JVA.

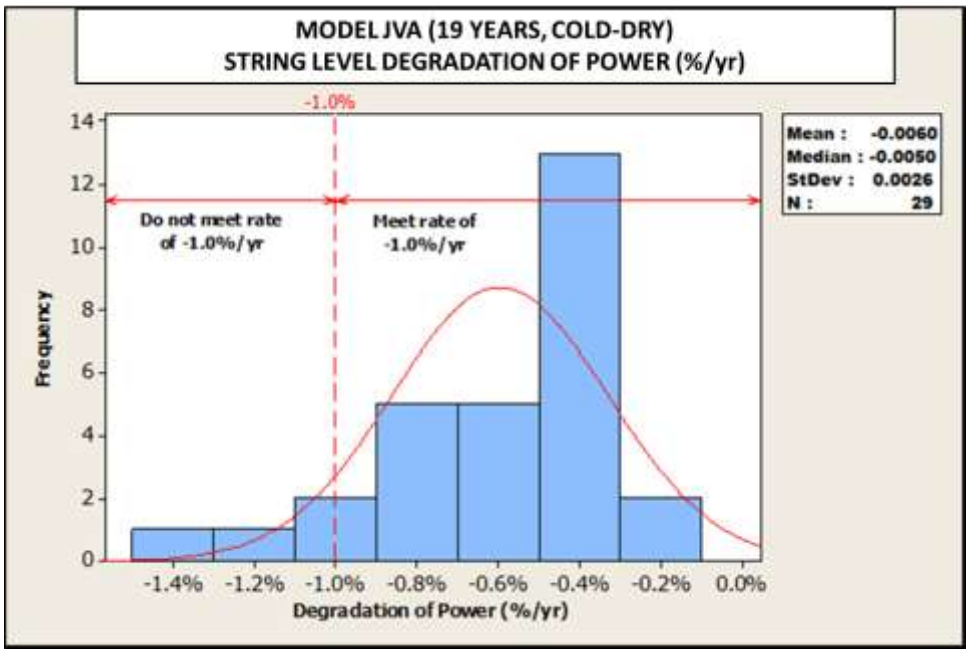

Figure 26 String Level Degradation for Model JVA

IV characterization was performed for 132 modules of the total 348 modules in the power plant, and their corresponding degradation rates were shown in Fig. 27. The modules from the disconnected string were excluded from the degradation evaluation. From this data, the average module-level degradation rate was determined to be 0.69%/year. The measured module level degradation is higher than string level degradation rates. This is due to the sample sizing where string level data has 100% CL, whereas 95% CL and 6.73% CI results in this variation.

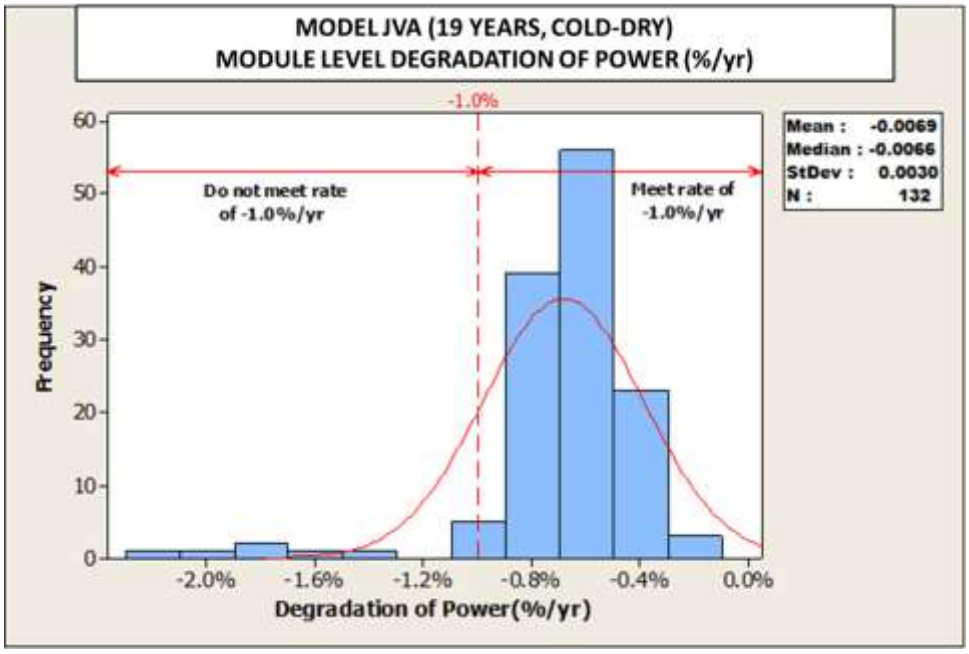

Figure 27 Module Level Degradation

Extrapolating the measured module degradation and including the safety failures, 89.6% of the modules are safe and are meeting the manufacturer's warranty, with only 6.1% of modules being safety failures and another 4.3% exceeding the manufacturer's warranty of 1%/yr. degradation rate. This is shown in Fig. 28 below.

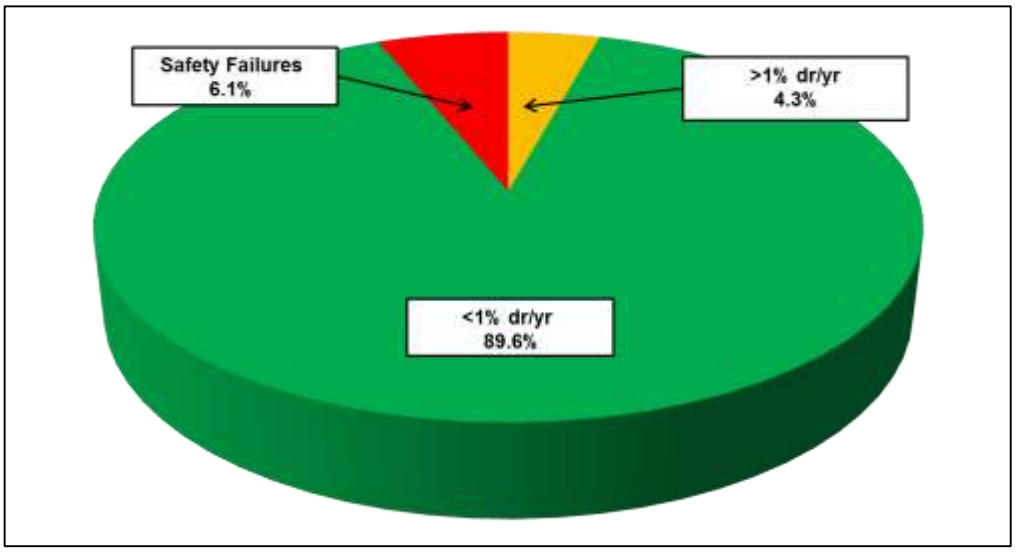

Figure 28 Model-JVA's safety failures and extrapolated degradation distribution

2.4.3. Occurrence and Detectability

Model JVA experienced 14 different failure/degradation modes. The occurrence ratings were assigned for these modes using count data to generate the frequency of occurrence. When failure modes backsheet delamination and backsheet scratches lead to exposing circuit, they were separated into a different failure mode to differentiate safety and degradation concerns. The count data for these failure/degradation modes were also separated accordingly. The broken module in the system belonged to the disconnected string, hence, given the count of zero. All the failure modes, with the exception of diode failure, were detected from visual inspection at the current site. Therefore, all these modes were given low ratings of 2, while diode failure required the usage of special instruments. Hence, it was given a higher rating of 4.

Table 11 Occurrence and Detectability

Defects	Count	Frequency (%)	CNF	Occurrence (O)	Detectability Criteria	Detection (D)
Backsheet Delamination	20	5.75	3.02	6	Visual Inspection	2
Backsheet Bubbles	86	24.71	13.01	8	Visual Inspection	2
Backsheet scratches	21	6.03	3.18	6	Visual Inspection	2
Near Edge Encapsulant delamination	30	8.62	4.54	6	Visual Inspection	2
Interconnect Discoloration	174	50.00	26.32	9	Visual Inspection	2
Encapsulant Browning	159	45.69	24.05	9	Visual Inspection	2
Cell Cracking	1	0.29	0.15	3	Visual Inspection	2

Over cell Encapsulant Delamination	115	33.05	17.39	8	Visual Inspection	2
Corrosion-like	18	5.17	2.72	6	Visual Inspection	2
No frame grounding	7	2.01	1.06	5	Visual Inspection	2
Burn marks on Cell Interconnect	2	0.57	0.30	3	Visual Inspection	2
Failed diodes (Open ckt)	6	1.72	0.91	4	Diode checker	4
Circuit exposed due to Backsheet delamination/ scratches	4	1.15	0.60	4	Visual Inspection	2
BackSheet Burns	2	0.57	0.30	3	Visual Inspection	2
Broken Glass	0	0.00	0.00	0	Visual Inspection	2

2.4.4. Severity

Severity of a failure mode is dependent on the effect of the failure mode if it affects the module performance or if it is a safety concern. The criteria for severity rating has been discussed in the previous section. The degradation rates were determined based on both string-level measured power as well as module-level measured power. The degradation rates based on the string-level measurement were assigned to all the modules in that particular string for calculating the severity for string-level RPN. While module level data was more appropriate, the collected data did not encompass all the failure modes observed in the field. So, module level degradation based severity ratings were

assigned for only those failure modes present in the modules for which IV measurements were taken.

	Based on Module IV data		Based on String IV data	
Defects	Degradation rate (%/Y)	Severity	Degradation rate (%/Y)	Severity
Backsheet Delamination	0.13	1	0.16	1
Backsheet Bubbles	0.29	1	0.24	1
Backsheet scratches	0.50	4	0.61	5
Near Edge Encapsulant delamination	0.15	1	0.11	1
Interconnect Discoloration	0.55	4	0.60	5
Encapsulant Browning	0.56	4	0.50	4
Cell Cracking	0.00	0	0.16	1
Over cell Encapsulant Delamination	0.42	3	0.50	4
Corrosion-like	0.33	3	0.29	1
No frame grounding	0.00	0	0.20	8
Burn marks on Cell Interconnect	0.12	8	0.24	8
Failed diodes (Open ckt)	0.10	10	0.53	10
Circuit exposed due to Backsheet delamination/ scratches	0.00	0	0.33	10
BackSheet Burns	0.14	8	0.34	8
Broken Glass	0.00	0	0.00	10

2.4.5. RPN Calculation

Using these ratings to generate the Risk Priority Number for each failure mode was implemented. The failure modes were divided into safety failure modes or performance failure modes based on which RPN was divided into safety RPN and performance RPN. Severity ranking is assigned based on degradation rates. The severity ranking was assigned to failure/degradation mode based on measured string level degradation rate and module level degradation rate. This, in return, results in String degradation based RPN

and Module degradation based RPN. The difference between String level RPN and Module level RPN arises only from severity.

To compare the RPN generated from string degradation data and module degradation data, the defects that are not included in module data have not been included in global RPN calculations. The RPN calculation is included in Table 12 and corresponding string Global RPN and Module Global RPN have been graphed in Fig. 29 and Fig. 30.

Table 12 RPN Calculation

Defects	**O**	**D**	Module S	Module-RPN	String S	String-RPN
Backsheet Delamination	6	2	1	12	1	12
Backsheet Bubbles	8	2	1	16	1	16
Backsheet scratches	6	2	4	48	5	60
Near Edge Encapsulant delamination	6	2	1	12	1	12
Interconnect Discoloration	9	2	4	72	5	90
Encapsulant Browning	9	2	4	72	4	72
Cell Cracking	3	2	0	0	1	6
Over cell Encapsulant Delamination	8	2	3	48	4	64
Corrosion-like	6	2	3	36	1	12
No frame grounding	5	2	0	0	8	80
Burn marks on Cell Interconnect	3	2	8	48	8	48
Failed diodes (Open ckt)	4	4	10	160	10	160
Circuit exposed due to Backsheet scratches	5	2	0	0	10	80
BackSheet Burns	3	2	8	48	8	48
Broken Glass	0	2	10	0	10	0

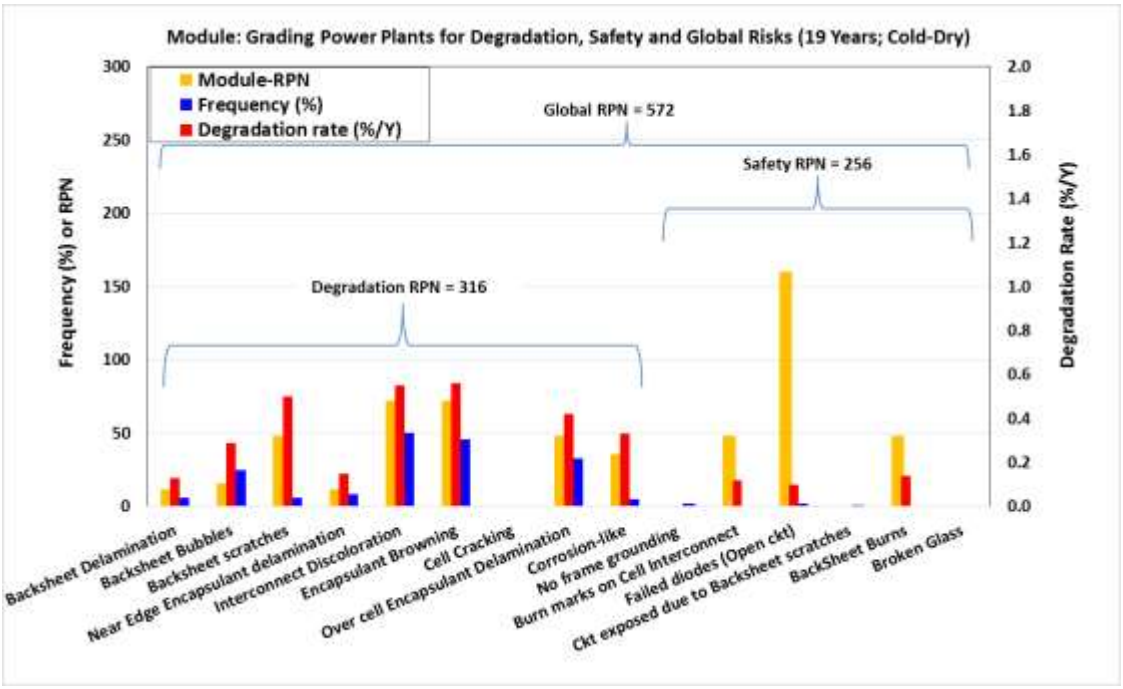

Figure 29 RPN - Module level for Model JVA

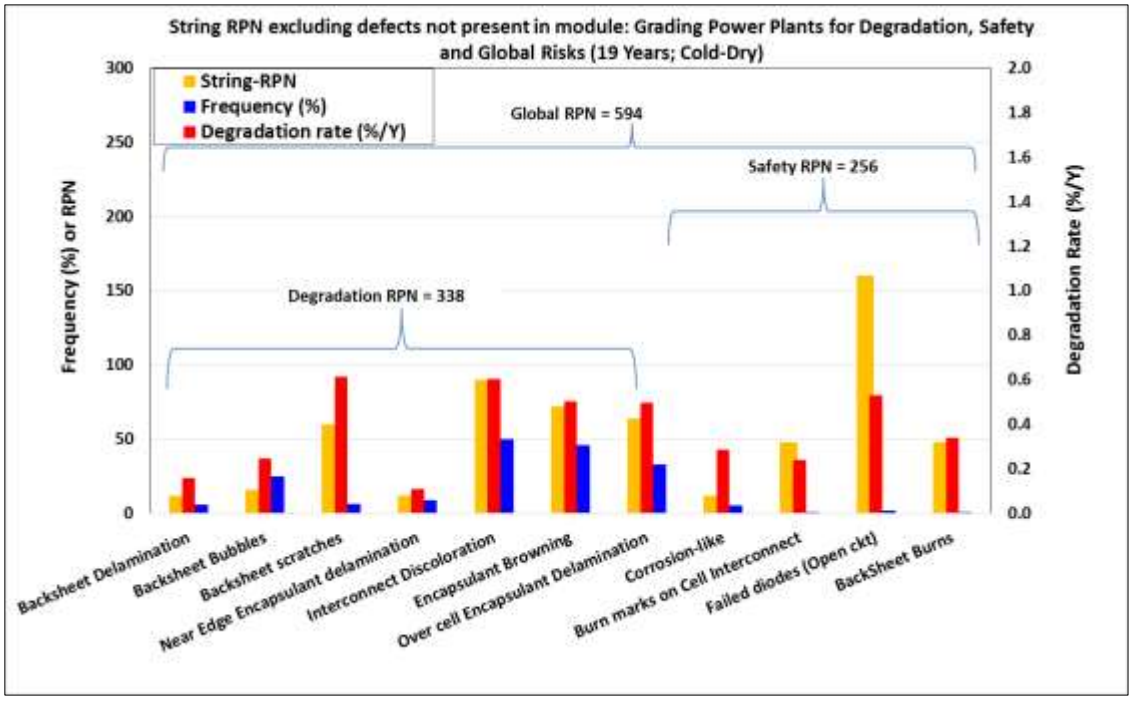

Figure 30 String Level RPN for Model JVA

The Global RPN generated with module level data is 572, whereas string level data is 594, indicating a negligibly small variation. This variation arises from degradation

RPN, which is justified as the string level performance in a culmination of modules in the string, thereby including a mismatch, if any, whereas module level is more specific. Hence, string level RPN can be used as an indicator for power plant performance when the mismatch factor is small. For the current Model JVA, not all the failure modes observed in the power plant were included in measured modules level IV data. Hence, string RPN, which includes all failure modes, is used to present the complete picture of failure modes as given in Fig. 31.

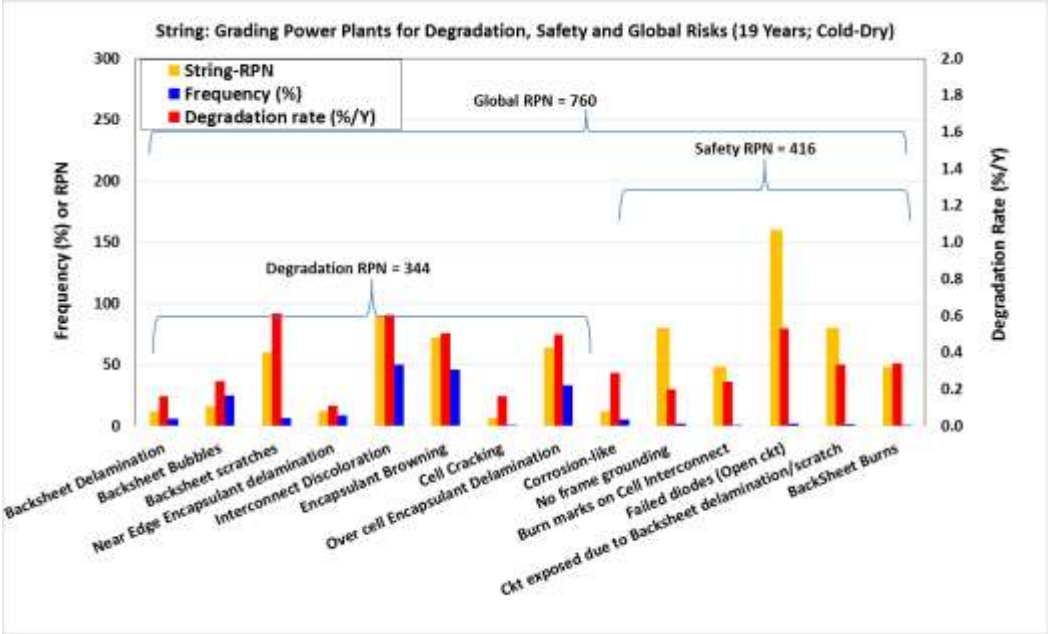

Figure 31 Global String level RPN with all defects for Model JVA

Model JVA has a Global RPN of 760, which is the sum of RPNs of all failures, of which 416 is safety RPN and the other 344 is due to degradation. Open circuited diode failure has the highest RPN, considering the fact that it is a safety failure and needs special equipment of Line Checker for detection. Of all the degradation modes, interconnect discoloration has the highest RPN, followed by encapsulant browning. Interconnect discoloration observed at this site is due to corrosion. This site has framed

modules and this, in combination with atmosphere moisture, leads to corrosion, thereby increasing series resistance. This increase in series resistance leads to local I^2R heating that could have caused the encapsulant browning.

2.4.6. Comparison with Model J

As indicated in the abstract, the statistical risk analysis of two power plants was jointly performed by two Masters students. Both power plants are located at the same cold-dry climate, but one power plant carries framed modules and the other carries frameless modules as shown in Fig. 32. This thesis presented the results on the framed modules. Comparing these two sites would help understand the failure modes and mechanisms for this climatic zone as both the plants had modules from the same manufacturer.

Table 13 Site Specification

	Model J	**Model JVA**
Size and Age	18 year	19 year
Module	120 W Frameless	120 W Framed
Dominant Failure Mode (degradation)	Over cell Encapsulant Delamination	Interconnect Discoloration and Encapsulant Browning
Degradation Rate (String level)	0.73% / year	0.6 % per yer
System overview	Functional	Not functional

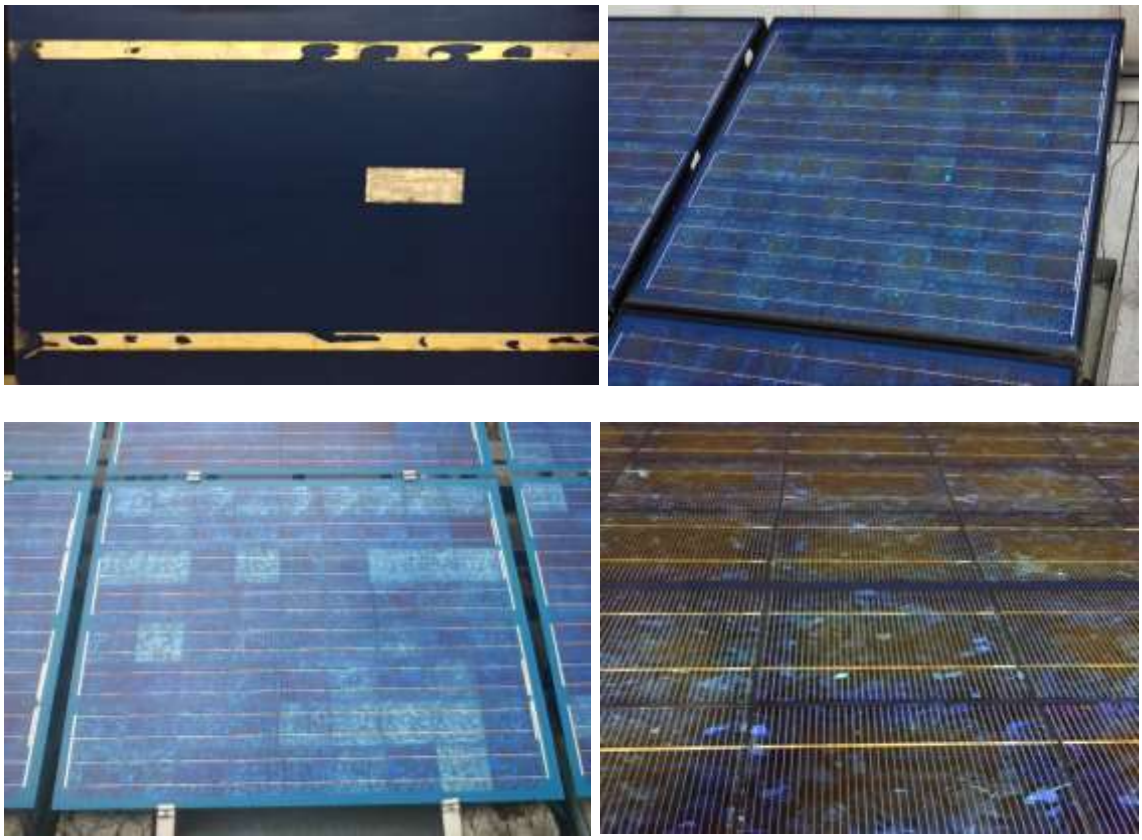

Figure 32 (clock-wise) a)Backrail mounting using adhesive of Frameless module Model-J b)Framed module at Model JVA; c) Encapsulant Browing and Interconnect Discoloration in Model JVA; d) Encapsulant Delamination in Model J;

The 18-year-old Model J has a string level mean degradation of 0.73%/year, which is more than 0.6% /year mean string degradation of the 19-year-old Model JVA. For both the sites, moisture ingress is the cause for degradation, however, the resultant dominant failure modes are encapsulant delamination and backsheet bubbles in Model J, while in Model JVA they are interconnect discoloration and browning as shown in Fig.33 and Fig.34 .

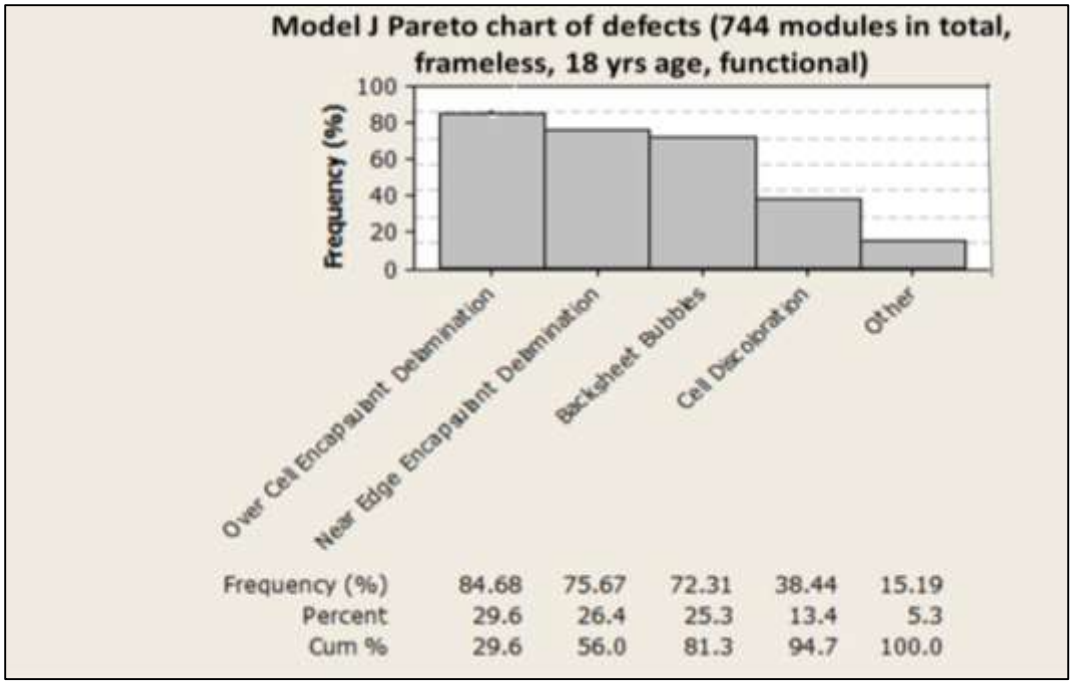

Figure 33 Pareto Chart for Model J

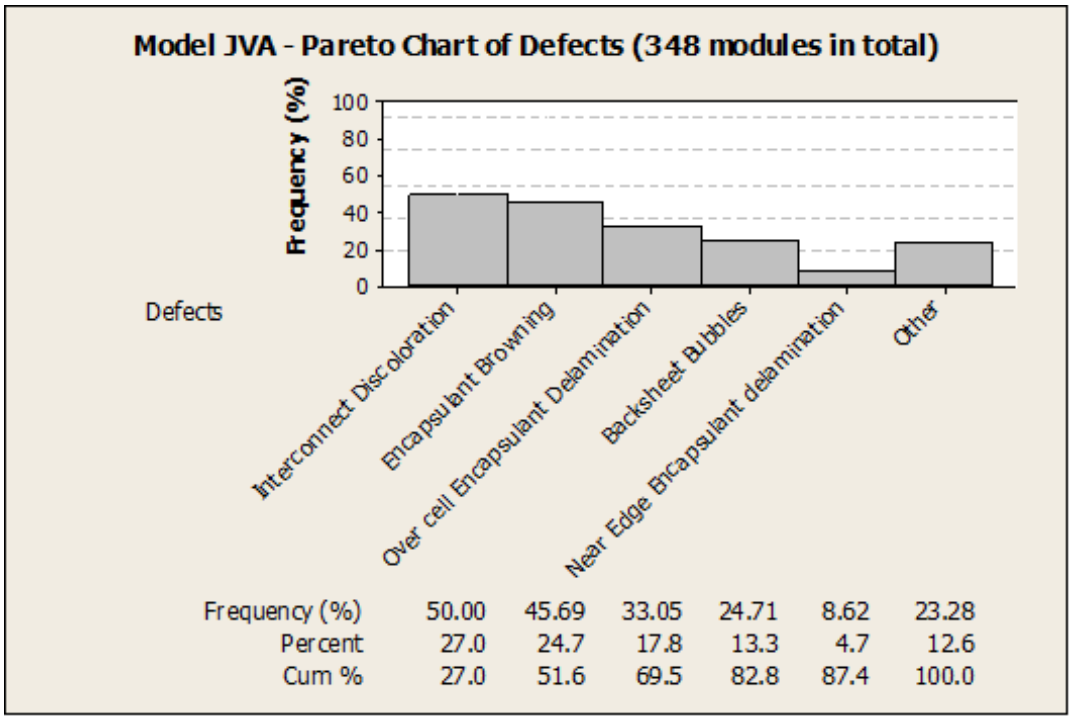

Figure 34 Pareto Chart for Model JVA

Considering they are in the same climate, similar age and from the same module manufacturer, one would expect similar failure and degradation modes for both frameless

(Model J) and framed (Model JVA). In the frameless modules of Model J, degradation is a result of the cascade effect caused by moisture penetration. The moisture ingress has lead to backsheet bubbles and delamination, and thereby causes encapsulant delamination. The encapsulant delamination, resulting in optical decoupling and, consequently, in I_{sc} loss, triggers one or more by-pass diodes leading to V_{oc} loss. Triggering of bypass diodes leads to over-heating over several years, and subsequently leads to more by-pass diode failures. On the other hand, in Model JVA electrolytic oxidation resulted in interconnect discoloration, and thereby encapsulant browning. This was not observed in Model J, as there is no leakage current in frameless modules. It was determined that V_{oc} loss is the highest contributing factor for degradation in Model J (frameless) due to encapsulant delamination. In Model JVA, Fill Factor loss due to interconnect electrolytic corrosion was the highest contributing factor. For the cold-dry climate, the Voc loss due to encapsulant delamination outweighs the Fill Factor loss of Model JVA, resulting in a higher degradation of Model J.

2.5.CONCLUSION

- Model JVA is a 19-year-old power plant in a cold-dry climatic condition, degrading at the rate of 0.6%/year. The module level and string level RPN can both be used to indicate power plant health if the mismatch effect is low.
- The Global RPN of the power plant can be divided into safety and degradation RPN. And degradation RPN can be used to identify the dominant degradation mode.
- For cold-dry climatic conditions, the degradation rate is about 0.6% per year (framed) to 0.73% per year (frameless).
- Encapsulant delamination was the dominant failure/degradation mode for frameless modules, while interconnect discoloration was the dominant degradation mode for framed modules. However, both these modes are the result of extent of moisture ingress.

REFERENCES

[1] T. Sarver, A. Al-Qaraghuli, and L. L. Kazmerski, “A comprehensive review of the impact of dust on the use of solar energy: History, investigations, results, literature, and mitigation approaches,” Renew. Sustain. Energy Rev., vol. 22, pp. 698–733, Jun. 2013.

[2] M. Mani and R. Pillai, “Impact of dust on solar photovoltaic (PV) performance : Research status , challenges and recommendations,” Renew. Sustain. Energy Rev., vol. 14, no. 9, pp. 3124–3131, 2010.

[3] H. W. A. Kimber, L. Mitchell, S. Nogradi, “The Effect of Soiling on Large Grid-Connected Photovoltaic Systems in California and the Southwest Region of the United States,” Conf. Rec. 2006 IEEE 4th World Conf. Photovolt. Energy Conversion, Waikoloa, HI, pp. 2391–2395, 2006.

[4] M. Gostein, B. Littmann, J. R. Caron, and L. Dunn, “Comparing PV Power Plant Soiling Measurements Extracted from PV Module Irradiance and Power Measurements,” no. 1, pp. 3004–3009, 2013.

[5] B. Knisely, “Angle of Incidence and Non-Intrusive Cell Quantum Efficiency Measurements of Commercial Photovoltaic Modules,” Arizona State University, 2013.

[6] B. Knisely, J. Kuitche, S. V. Janakeeraman, and G. Tamizhmani, “Validation of Draft International Electrotechnical Commission 61853-2 Standard : Angle of Incidence Effect on Photovoltaic Modules Solar America Board for Codes and Standards,” A report of Solar America Board for Codes and Standards (solarabcs.org), 2013.

[7] D. L. King, "Measuring Angle of Incidence (AOI) Influence on PV Module Performance," Private communication (this document is available in Appendix A of Reference 5), June 2012.

[8] International Electrotechnical Commission (IEC) 61853-2 (Draft), "Photovoltaic (PV) Module Performance Testing and Energy Rating - Part 2: Spectral Response, Incident Angle, and Module Operating Temperature Measurements," May 2012.

[9] J. John, V. Rajasekar, S. Boppana, S.Tatapudi, G. TamizhMani, “Angle of Incidence Effects on Soiled PV modules”, SPIE Conference, San Diego, August 2013.

[10] G. Kuitche, Joseph;TamizhMani, "Accelerated Lifetime Testing of Photovoltaic Modules Solar America Board for Codes and Standards," A report of Solar America Board for Codes and Standards (solarabcs.org), 2013.

[11] J. K. Mallineni, "Failure and Degradation Modes of PV modules in a Hot Dry Climate: Results after 4 and 12 years of field exposure," Arizona State University, 2013.

[12] K. R. Yedidi, "Failure and Degradation Modes of PV modules in a Hot Dry Climatic: Results after 16 years of Field Exposure," Arizona State Univesity, 2013.

[13] S. Shrestha, "Determination of Dominant Failure Modes Using Combined Experimental and statistical Methods and Selection of best method to calculate Degradation Rates," Arizona State University, 2014.

[14] J. Wohlgemuth, D. W. Cunningham, and A. Nguyen, "Failure Modes of Crystalline Si Modules."

[15] J. M. Kuitche, R. Pan, and G. Tamizhmani, "Investigation of Dominant Failure Mode (s) for Field-aged Crystalline Silicon PV Modules under Desert Climatic Conditions," 2013.

APPENDIX A

STANDARD OPERATING PROCEDURE (SOP) FOR DUST SAMPLING USING WASHABLE LINT ROLLERS

Applications

This procedure shall be used in all indoor and outdoor dust sampling from the top surface of the solar modules.

Procedure

1- Using a microbalance, measure the mass of the roller and write it down as **m1** in Table 1.

2- Put the roller in the Ziploc bag, seal the bag well, and mark it.

3- If it is outdoor sampling, do it after 10:00 a.m. To start sampling, take the roller out of the bag and roll it on a predefined sampling area (A) within the top surface of the solar module. Roll it both vertically and horizontally as shown below. Write down the sampling area **(A)** in Table 1.

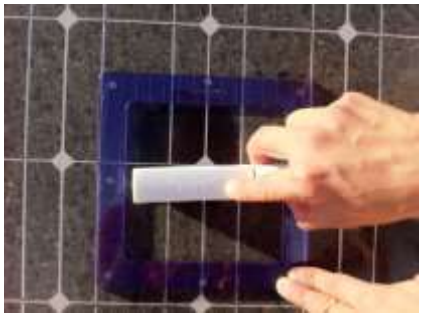
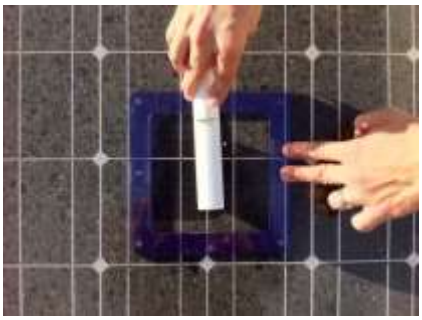

4- Immediately after sampling, put the roller back into the Ziploc bag and seal it very well.
5- Again, using the microbalance, measure the mass of the roller after sampling, and write it down as **m2** in Table.1.
6- Using Table 1, calculate the soiling density for sample 1 **(SD1)**.
7- Do the same above steps again for samples 2, 3, and 4 to get **SD2, SD3, and SD4**, respectively.
8- Complete filling out Table 1 to get the Average Soiling Density **(ASD)**.

Table.1 Calculating the Average Soiling Density (ASD) from the dust samples

Sample 1		
m1 (g)=	m2 (g)=	A (cm^2)=
SD1 (mg/m^2)= $10^7 \times \frac{m2-m1}{A} =$		
Sample 2		
m1 (g)=	m2 (g)=	A (cm^2)=
SD2 (mg/m^2)= $10^7 \times \frac{m2-m1}{A} =$		
Sample 3		
m1 (g)=	m2 (g)=	A (cm^2)=
SD3 (mg/m^2)= $10^7 \times \frac{m2-m1}{A} =$		
Sample 4		
m1 (g)=	m2 (g)=	A (cm^2)=

SD4 (mg/m^2)= $10^7 \times \frac{m2-m1}{A} =$
Average Soiling Density (ASD) - for all above samples
SD1 (mg/m^2)= SD2 (mg/m^2)= SD3 (mg/m^2)= SD4 (mg/m^2)=
ASD (mg/m^2)= $\frac{SD1+SD2+SD3+SD4}{4} =$

Notes

To reuse the rollers, wash with warm water and dish soap, and then let dry (put in the oven on 30°C for 3 hours).

APPENDIX B

STANDARD OPERATING PROCEDURE FOR REFLECTANCE AND TRANSMITTANCE

Applications

This procedure shall be used in all indoor and outdoor Reflectance and Transmittance measurements using HandHeld FieldSpec 4 Wide-Res spectroradiometer.

Procedure - Reflectance

1. In the rear portion of the spectroradiometer unit, connect the power supply to the input 12 VDC port. Also, connect the Ethernet cable to the appropriate port with the other end connected to the laptop. (Ensure that the laptop is always switched on after the spectroradiometer.)

2. Connect the accessory power port to the contact probe as shown below.

3. To connect the fiber optic, first remove the screws in such a manner that the grey color screw is placed in the same place. Then take the fiber optic and insert it in the screw that has been removed. Gently push the fiber optic in the place were the screws were already present and tighten it. **(Handle the fiber optic with utmost care as it is sensitive and tends to break.)**

4. Hit the ‘ON’ button, which is on the rear side of the spectroradiometer unit, and then click the ‘ON’ button that is present on the contact probe so that the instrument starts warming up. For reflectance measurements, the light source should be switched on for a minimum of 15 minutes, whereas, for radiometric measurements, the time is extended to an hour.

5. Even for outdoor measurements, initially use the power supply as the source and then once the instrument is warmed up, the battery can be used. The battery is charged separately by connecting one end of the power cord to the battery and the other end to the supply. As in step 1, instead of connecting the power supply to 12VDC, connect the battery in its place.

6. Once the instrument is warmed up, take a small square-shaped, black colored cardboard/sheet and make a circle in the center the same as the size of the lens. Insert it to avoid the entry of the stray light and then clean the lens using lens wipes (Isopropyl alcohol and a soft cloth). Switch on the laptop.

OPTIMIZATION AND WHITE REFERENCE:

Before taking any reading, first you need to optimize the instrument to the current atmospheric conditions. (If you are doing an outdoor experiment, take the instrument outdoors and optimize it, as the indoor and outdoor atmospheric conditions differ). Optimize the instrument whenever the atmospheric conditions

differ or whenever a beep sound comes from the instrument indicating that the instrument is saturating.

1. Cover the lens of the contact probe using white reference (WR). Never touch the central white portion of the WR as it is already calibrated. Then hit the RS^3 software in the desktop. (There are two RS^3 software in the desktop; click high contrast for outdoor measurements).

2. A dialog box appears. Using the drop down menu, change the settings to Bare fiber and raw DN mode. Then hit the ‘OPT’ (Optimize) to go ahead with the optimization.

3. Once optimization is done, then click the ‘WR’ (White Reference) which is right next to the ‘OPT’. After collecting the WR, you get an image as below. A straight line appears at reflectance 1, indicating that the spectroradiometer unit has reflected all the light that it has encountered.

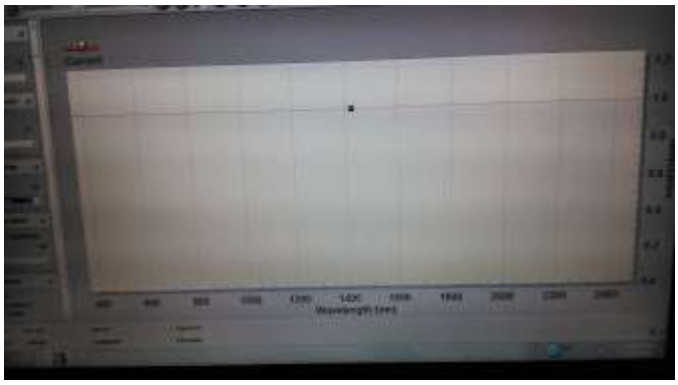

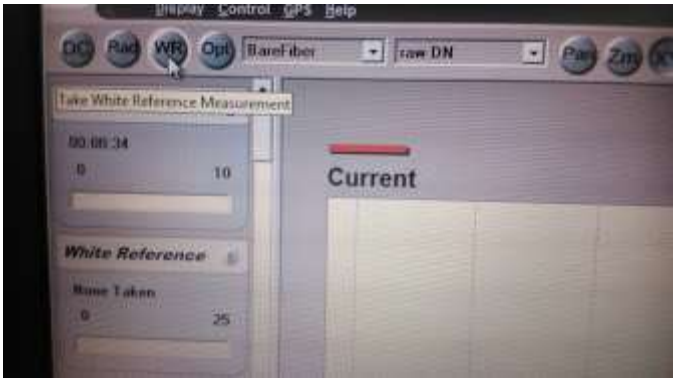

DATA COLLECTION:

Then the WR cap is removed and the contact probe is placed perpendicular to the sample for which the reflectance measurements are to be made. For saving the measurements, go to Control -> Spectrum save -> Dialog box appears -> Give the file name and check for the dates -> Hit Begin Save. The measurements start saving and for each and every spot on the sample you will have 10 readings.

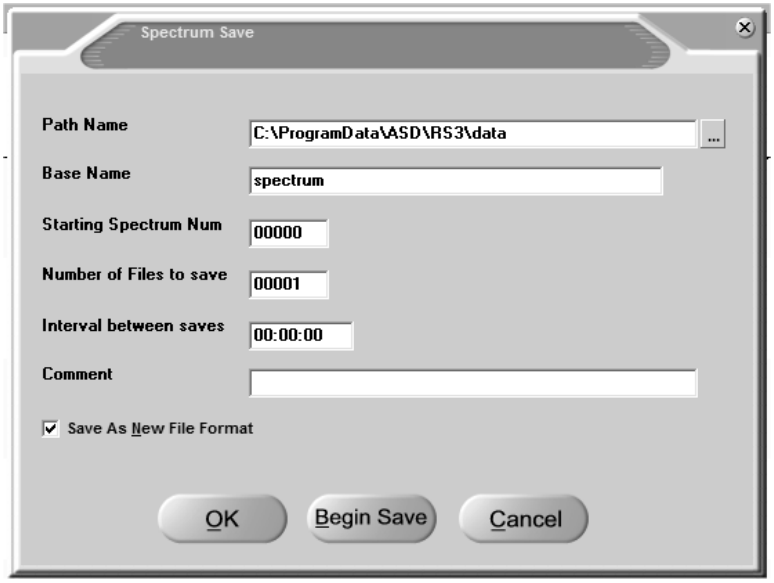

CONVERSION OF ASD TO TXT FILES:

Once all the measurements are done, the reflectance values are saved as ASD files and the next step is to convert them to TXT files. Go to ViewSpec Pro -> File -> Open (open the files you want to convert) -> Process -> ASCII Export -> In the dialog box, just change the Data for .asd files only to Reflectance (don't change any) -> OK.

The Output path where the processed data gets stored is indicated at the bottom of this software.

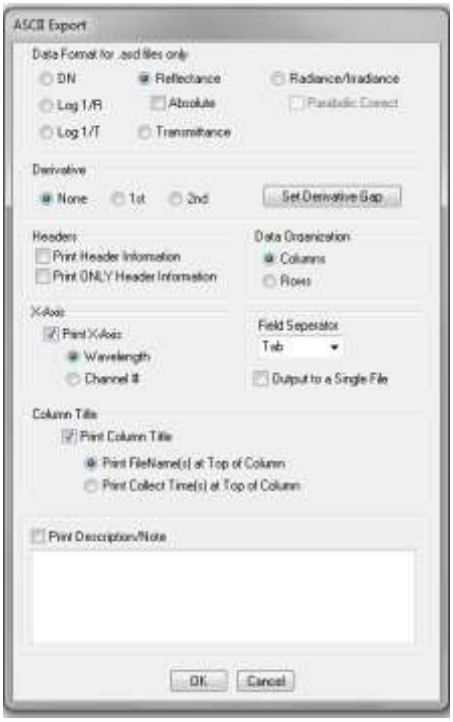

NOTE: For any further information about the Spectroradiometer, click on the below link to access the user manual;

http://support.asdi.com/Document/Viewer.aspx?id=140

Procedure – Transmittance

1. In the rear portion of the spectroradiometer unit, connect the power supply to the input 12 VDC port. Also, connect the Ethernet cable to the appropriate port and the other end to the laptop, similar to reflectance measurements. (Ensure that the laptop is always switched on after the spectroradiometer.)

2. Ensure that the bare fiber is connected to RCR. (When the bare fiber is inserted into the RCR, make sure that you hear a click).
3. Hit the ‘ON’ button which is on the rear side of the spectroradiometer unit and then click the ‘ON’ button that is present on the contact probe so that the instrument starts warming up. For radiometric measurements, the recommended warm up time is about one hour.

4. Even for outdoor measurements, initially use the power supply as the source and then once the instrument is warmed up, the battery can be used. The battery is charged separately by connecting one end of the power cord to the battery and the other end to the supply. As in step 1, instead of connecting the power supply to 12VDC, connect the battery in its place.

Optimization and Radiometric Calibration

1. There are two versions of ASD data collection software: RS^3 and RS^3 – high contrast. Both the versions work similarly except for the fact that high contrast version is built with higher contrast for ease of use in bright ambient conditions. Both the programs open software with the following layout.

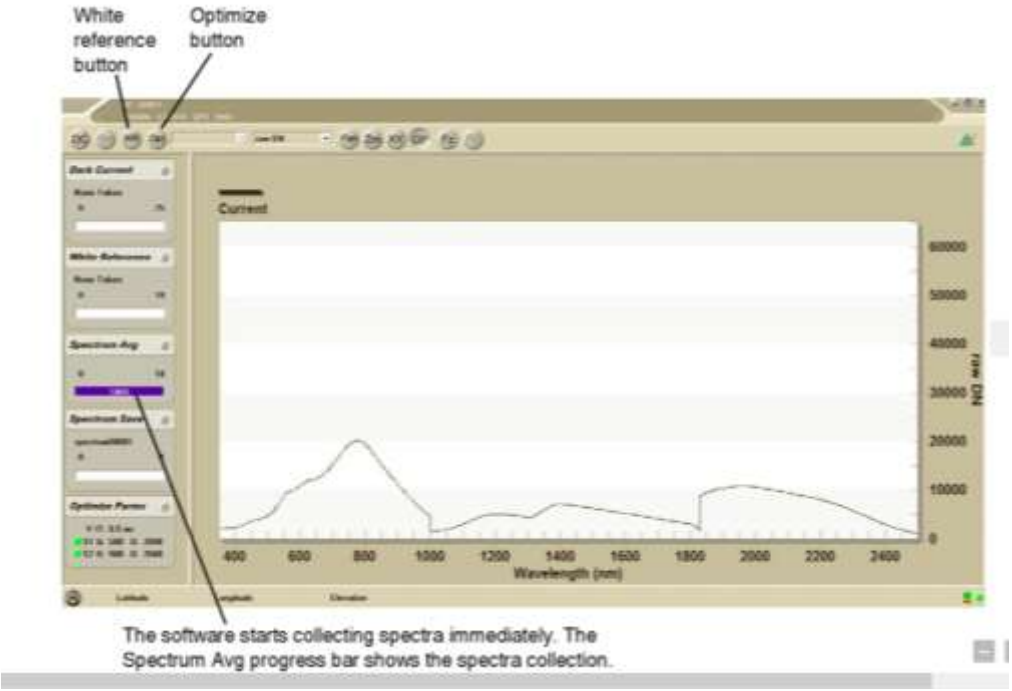

a. **Foreoptic selection**: Choose Menu option: CONTROL>ADJUST CONFIGURATION>foreoptic selection RCR

OR this can be done on the screen in the drop down menu beside OPT button>Select RCR

b. **Optimization and 'Rad'**: The instrument needs to be optimized with changing ambient conditions. Optimizing every 10 minutes under field conditions is recommended. If outdoor measurements are to be done, optimize it outdoors and not indoors as the ambient conditions differ. Click OPT on the screen OR CTRL O. While optimizing, the foreoptic or RCR should be pointed at the brightest area to be measured at the maximum illumination condition. After optimization, press on 'RAD' to collect irradiance sprectra.

c. **Saving spectrum**: Choose menu option: CONTROL>SAVE SPECTRUM The following window will open and each time spectrum is taken, 10 iterations are taken. This can be changed but it's recommended to take 10 iterations.

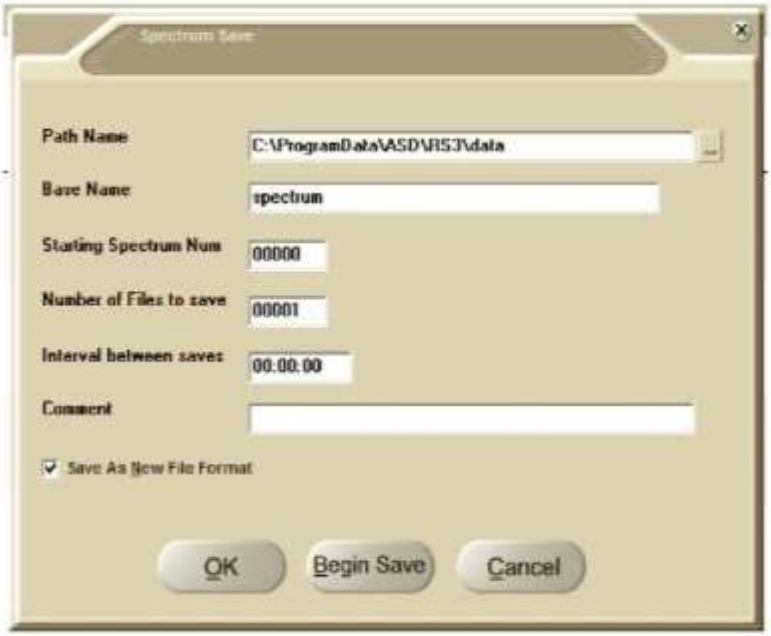

Path name: Location where the data will be saved.

Base name: Name of the data collected

Starting number: Start number (00000 generally)

Number of files: Number of spectrums to be collected (10 recommended)

Interval: 0

HIT BEGIN SAVE TO START COLLECTING SPECTRUM or else HIT OK, and later enter on the spacebar whenever you need to start collecting the spectrum

CONVERSION OF ASD TO TXT FILES:

Use ViewSpec™ Pro software to view and post process the saved spectra. The Transmittance values are saved as ASD files and the next step is to convert them to the TXT files. Go to ViewSpec Pro -> File -> Open (open the files you

want to convert) -> Process -> ASCII Export -> In the dialog box, just change the Data for .asd files only to Radiance/Irradiance (don't change any) -> OK.

The Output path where the processed data gets stored is indicated at the bottom of this software.

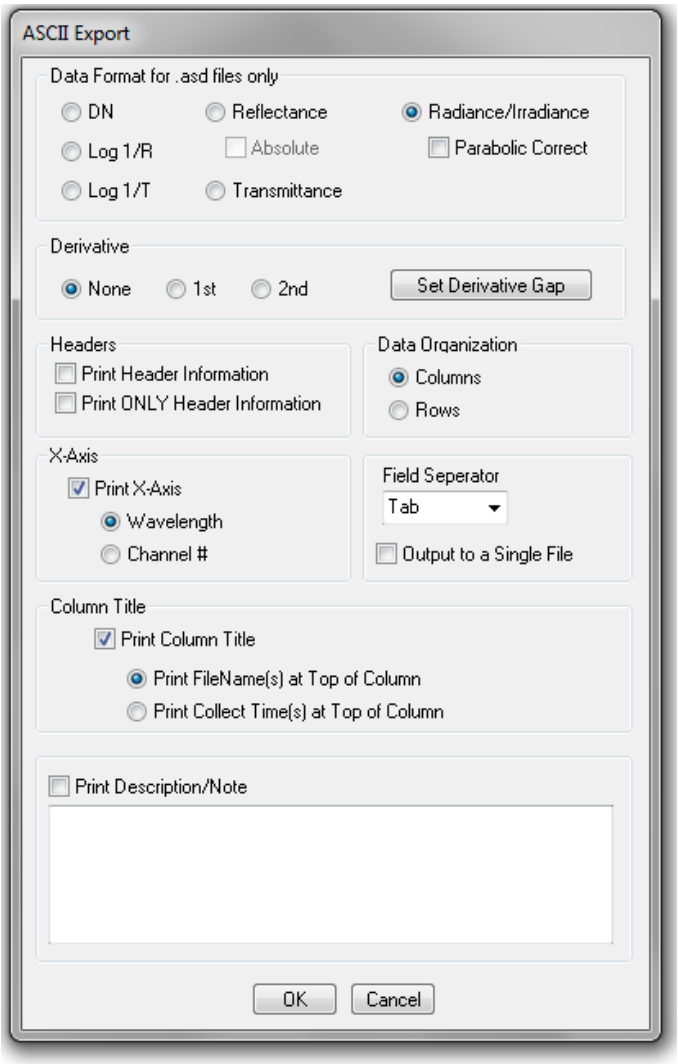

APPENDIX C

Reflectance spectra for all technologies at all soil densities for reference.

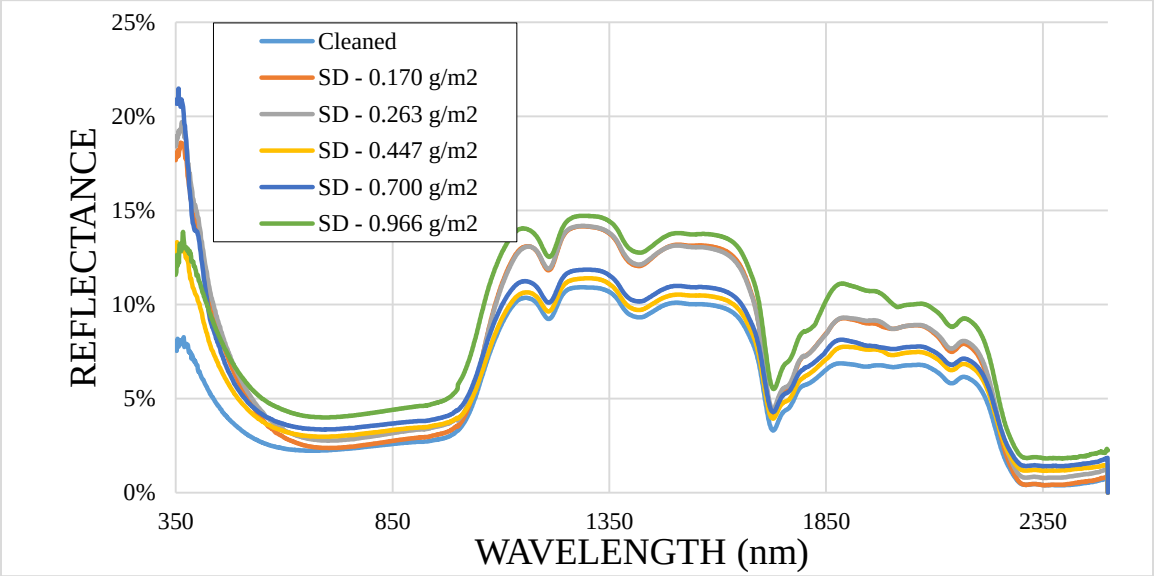

Figure 1. Reflectance Spectrum for different soil densities for Poly Si.

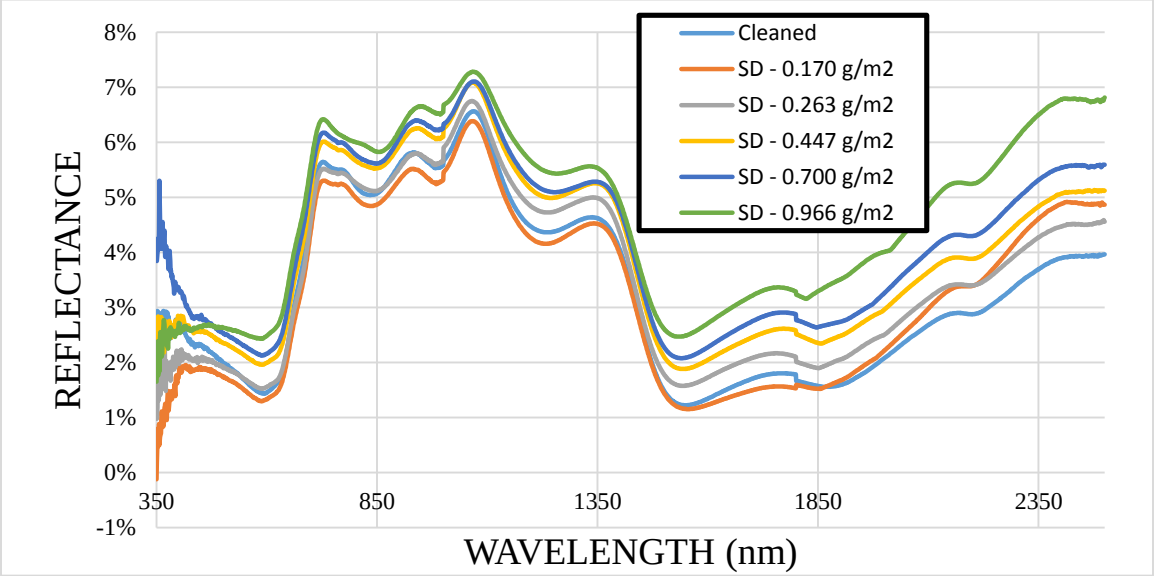

Figure 2. Reflectance Spectrum for different soil densities for A Si.

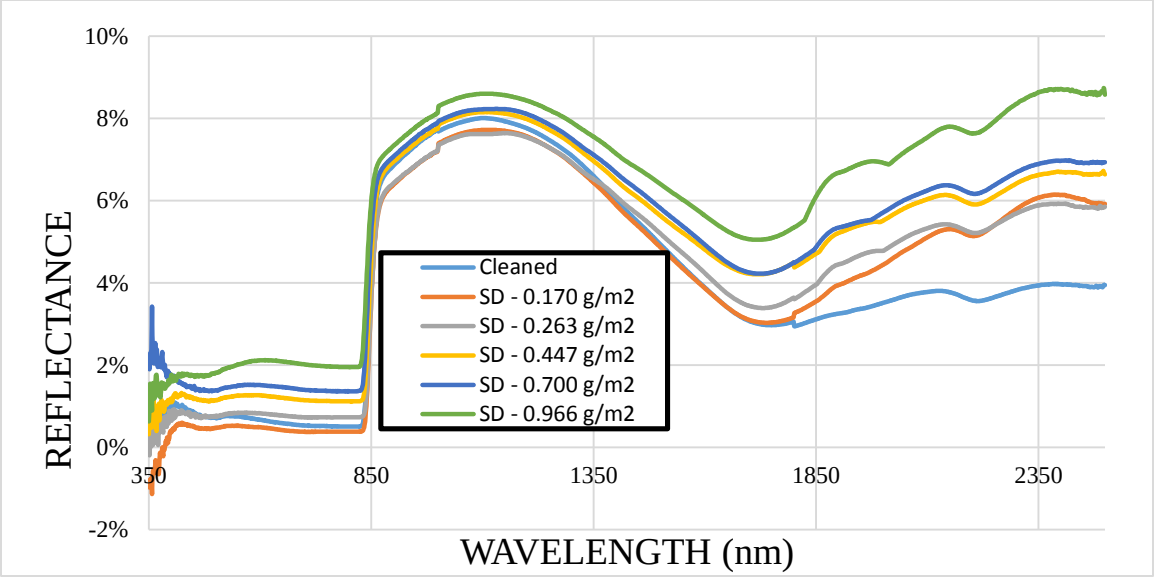

Figure 3. Reflectance Spectrum for different soil densities for CdTe.

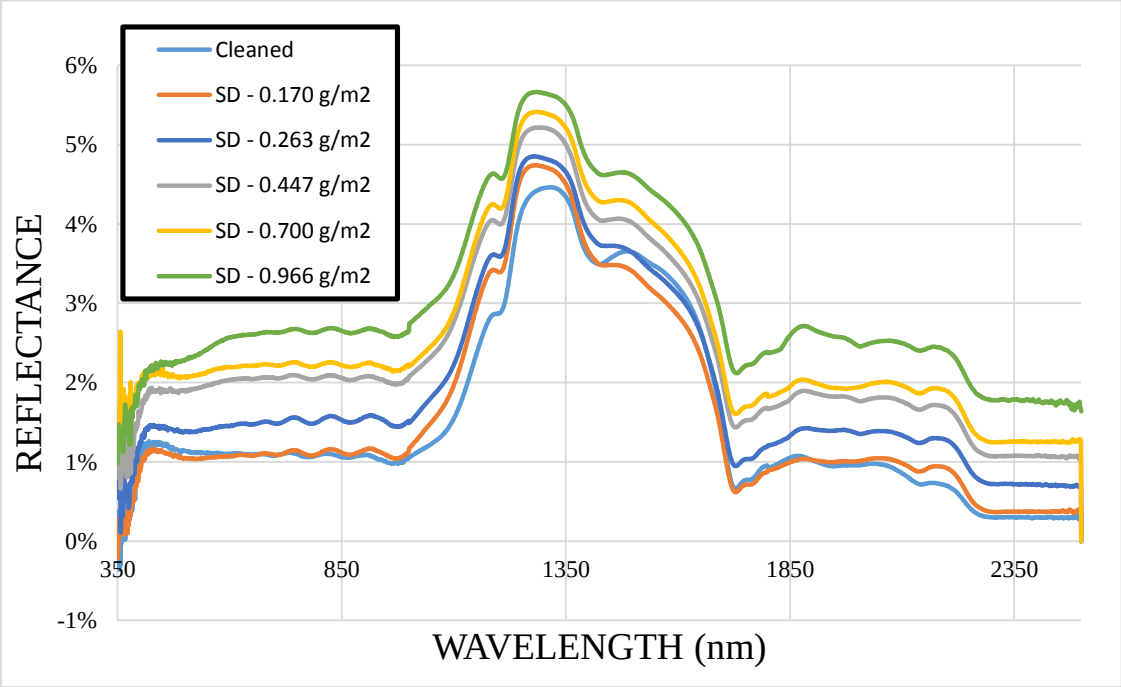

Figure 4. Reflectance Spectrum for different soil densities for CIGS.

Delta Plots (Reflectance Difference) for all technologies

Reflectance Difference is the difference between cleaned and soiled module reflectance.

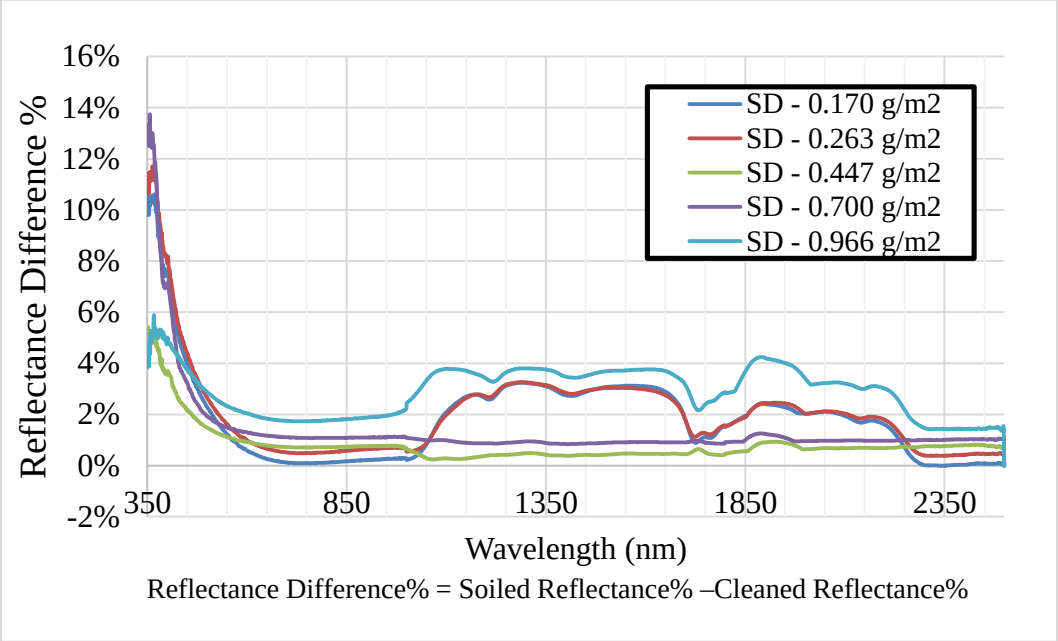

Figure 5. Reflectance Spectrum for different soil densities for Poly Si.

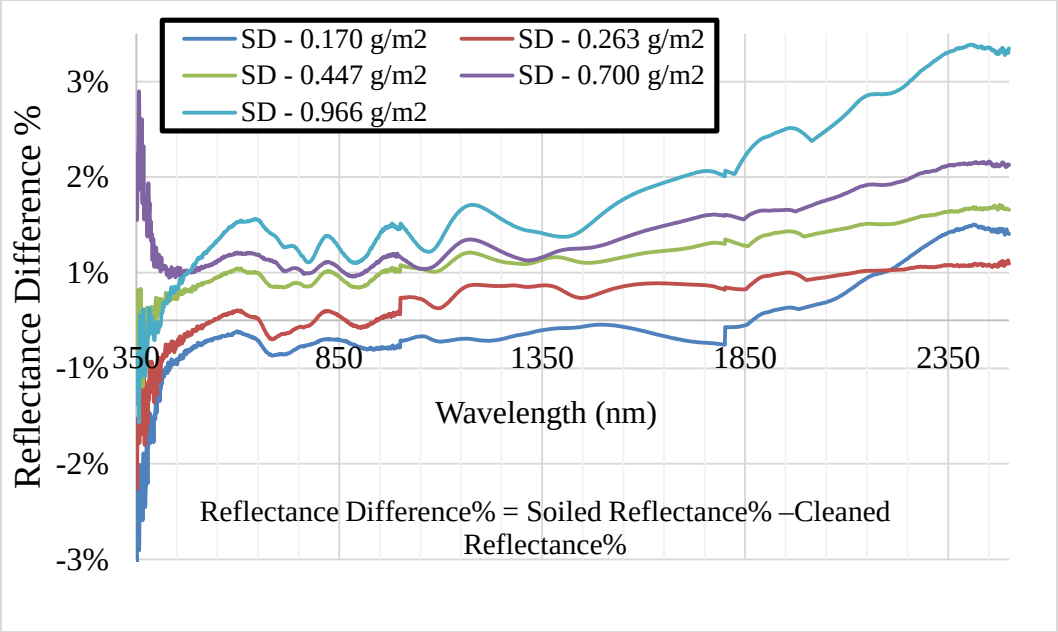

Figure 6. Reflectance Spectrum for different soil densities for a Si.

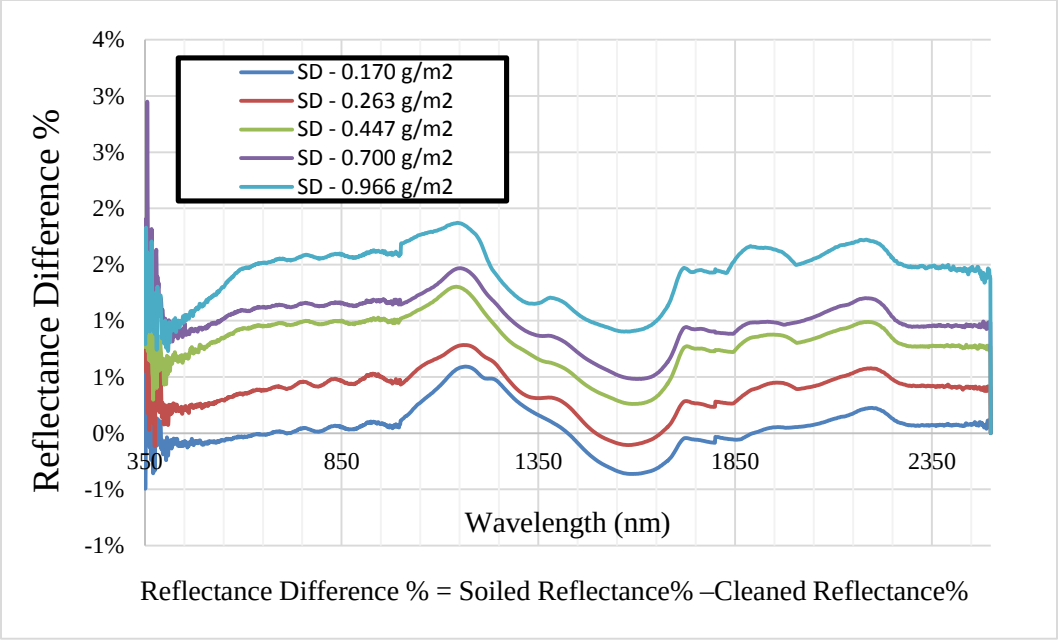

Figure 7. Reflectance Spectrum for different soil densities for CIGS.